PROPERTIES OF γ-RAY TRANSITIONS IN ^{33}S AND ^{35}S

by

James David Hutton

Department of Physics
Duke University

Date April 12, 1974

Approved:

N. Russell Roberson, Supervisor

Dissertation submitted in partial fulfillment of the requirements for the degree of Doctor of Philosophy in the Department of Physics in the Graduate School of Duke University

1974

ABSTRACT

(Physics)

PROPERTIES OF γ-RAY TRANSITIONS IN ^{33}S AND ^{35}S

by

James David Hutton

Department of Physics
Duke University

Date: _____

Approved:

_____

N. Russell Roberson, Supervisor

_____

_____

_____

_____

An abstract of a dissertation submitted in partial fulfillment of the requirements for the degree of Doctor of Philosophy in the Department of Physics in the Graduate School of Duke University

1974

PROPERTIES OF γ-RAY TRANSITIONS IN ^{33}S AND ^{35}S

by

James David Hutton

The properties of γ-ray decays of low-lying levels in ^{33}S and ^{35}S have been studied via the $^{32,34}S(\vec{d},p\gamma)^{33,35}S$ reactions. Multipole mixing ratios have been measured for γ-ray transitions between bound levels with particle-γ-ray angular correlations and Method II of Litherland and Ferguson. This is one of the first uses of a very powerful polarized beam technique developed and first used at TUNL (68) which allows the extraction of information not previously possible with the (d,pγ) reaction. A tensor polarized deuteron beam from the TUNL Lamb-shift polarized ion source accelerated to 4.72 MeV with the TUNL FN Tandem accelerator was used to bombard 80 $\mu g/cm^2$ natural sulfur and enriched (90%) ^{34}S targets prepared by evaporating sulfur onto a gold foil then evaporating gold on top. Four 7.6 x 7.6 cm NaI(Tl) scintillation detectors situated at angles between 30° and 90° to the beam detected γ-rays in coincidence with protons detected at 180° in a 2 mm thick annular surface barrier detector. Results for ^{33}S are compared with previous results (5) with which they agree well, and with current shell-model theory. Mixing ratios have been measured for many levels in ^{35}S as follows(E_x : J^π : δ): (1991:7/2$^-$:0.042), (2348:3/2$^-$:0.044), (2718:(3/2$^+$):0.065,-5.4), (2718:(5/2$^+$):-0.36,-7.1), (2935:(3/2):0.34), (2935:(5/2):0.086), (3802:3/2$^-$:0.18, -8).

ACKNOWLEDGEMENTS

I would like to express my gratitude to my advisor Dr. N. R. Roberson for his help, support and encouragement during this project. I would like to thank Dr. D. R. Tilley and Dr. C. R. Gould for their many helpful discussions concerning the experimental apparatus and analysis. I am indebted to Dr. T. B. Clegg for his extensive help in the operation and understanding of the polarized ion source. I wish to thank Dr. C. E. Busch and Dr. T. A. Trainor for their help in the operation of the polarized ion source.

I would like to express my appreciation to Mr. E. C. Hagen, Mr. J. R. Williams and Mr. R. Ledford for their assistance in various tasks and in taking data. I would like to express my sincere appreciation to the entire technical staff of the Laboratory for their continued and invaluable assistance in the operation and maintenance of the experiment. Thanks are due to Mr. A. W. Lovette and the Instrument Shop for their expert fabrication of parts of the experimental apparatus.

I am grateful to Dr. H. W. Newson and Dr. E. G. Bilpuch and the Nuclear Structure Laboratory for providing me with the research assistantship that allowed me to complete this work.

I would like to thank my parents for their interest and encouragement. I would especially like to thank my wife Sue for her love, encouragement and interest.

This project was supported in part by the U. S. Atomic Energy Commission.

CONTENTS

LIST OF FIGURES

LIST OF TABLES

PROPERTIES OF γ-RAY TRANSITIONS IN ^{33}S AND ^{35}S

Chapter I

INTRODUCTION

The nuclei ^{33}S and ^{35}S are in a region of the s-d shell that has been studied very extensively both experimentally (1-34) and theoretically (49-63). Theorists have had considerable success in applying various forms of theoretical models to many nuclei in this mass region. Recently shell model approaches based on the modified surface delta interaction (MSDI)(50-63) have had great success in explaining many features of nuclei in the region A=30-35. In particular, two recent calculations (51,52) are of immediate interest to the present case.

The study of γ-ray transitions of nuclei can allow the measurement of properties of the nucleus without the uncertainties of interaction theories. As will be shown later, reaction matrix elements which involve nuclear wave functions connected by only the electromagnetic operator can be determined experimentally. These allow a more critical comparison of theory and experiment than would be the case where reaction theories were involved.

The nucleus ^{33}S has been the subject of intensive experimental investigation for several years (1-23) and the known J^{π}, mean lives, δ, etc. of the low lying levels has provided much information for comparison with theory. The electromagnetic properties in particular have been studied via the $(\alpha,n\gamma)$ reaction (5), a reaction ideal for determining both lifetimes and

mixing ratios.

The nucleus ^{35}S is much less accessible to study than ^{33}S. The targets require enriched isotope and few reactions can be employed. The nucleus has been studied most often via the $^{34}S(d,p\gamma)^{35}S$ reaction (and (d,p) reaction) with the result that many ℓ_n values have been determined (26). The $(\alpha,n\gamma)$ reaction, however, cannot be used to populate ^{35}S. As a result only a few multipole mixing ratios are known for this nucleus. The work already done with the (d,p) reaction plus the known lifetimes for many low-lying states means that mixing ratios are the parameter needed for calculations of the transition matrix elements. The mixing ratio determines the relative strengths of competing transition matrix elements and provides a critical test of shell model theory.

In the present investigation the levels of ^{35}S were studied with the $^{34}S(\vec{d},p\gamma)^{35}S$ reaction. A new technique proposed by McCullen and Seyler(42) for measuring particle-γ-ray angular correlations and first developed at the Triangle Universities Nuclear Laboratory was used. This method utilizes a tensor polarized deuteron beam from the TUNL Lamb-shift polarized ion source and a co-linear geometry to restrict the magnetic substate population of the excited states of the residual nucleus. (see Section II. C. 1) Since many mixing ratios have been measured (5) for ^{33}S, the $^{33}S(\vec{d},p\gamma)^{35}S$ was also used in this work to study the low-lying levels of ^{33}S. In this way the previous results for ^{33}S have been confirmed and the new technique described in this work has been thoroughly tested.

Chapter II

PROCEDURE

A. Apparatus

1) Polarized ion source

The deuteron beam for this experiment was generated by the TUNL Lamb-shift polarized ion source(46) which is capable of generating beams of vector polarized protons and vector and tensor polarized deuterons. The Lamb-shift source relies on the atomic structure of the hydrogen (deuterium) atom, as shown in Figure 2. Certain substates of the metastable 2S atoms are eliminated by inducing transitions to the 2P excited state and hence to the ground state. The remaining 2S substates are selectively charge-excharged and accelerated.

As shown in Figure 1, a positively charged beam is extracted from the duo-plasmatron ion source and decelerated to 1100 eV energy. It then enters the cesium charge exchange canal where part of the beam becomes electrically neutral with one electron in the 2S metastable state. After passing through a transverse E-field which sweeps out the remaining charged beam, the neutral atoms enter the spin filter. The spin filter consists of a longitudinal magnetic field, a transverse DC E-field, and an RF E-field(1609 MHz). The magnetic field induces Zeeman splitting of the magnetic substates as shown in Figure 2, and is adjusted to cause the 2S levels with electron spin projection $M_J = -1/2$ to overlap the 2P states. The transverse DC E-field causes Stark mixing of these overlapping levels, inducing transitions from the 2S to the 2P levels, which then decay by dipole radiation to the ground state. The RF E-field is used in a subtle

5

Figure 1. Schematic diagram of polarized ion source layout.

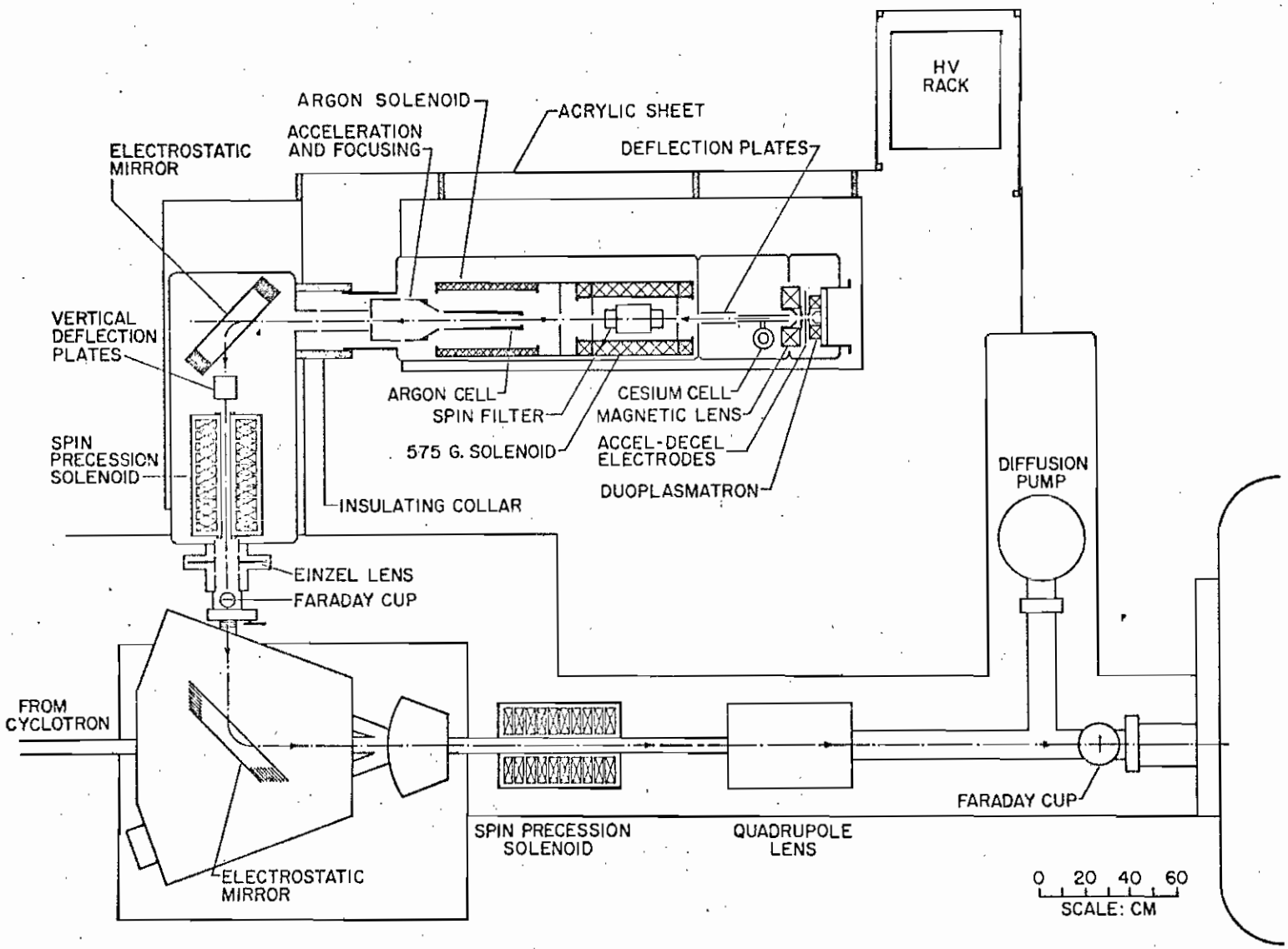
HV
RACK
ARGON SOLENOID
ACRYLIC SHEET
ACCELERATION
AND FOCUSING
ELECTROSTATIC
MIRROR
DEFLECTION PLATES
VERTICAL
DEFLECTION
PLATES
ARGON CELL
SPIN FILTER
575 G. SOLENOID
CESIUM CELL
MAGNETIC LENS
ACCEL-DECEL
ELECTRODES
DUOPLASMATRON
SPIN
PRECESSION
SOLENOID
INSULATING COLLAR
DIFFUSION
PUMP
EINZEL LENS
FARADAY CUP
FROM
CYCLOTRON
ELECTROSTATIC
MIRROR
SPIN PRECESSION
SOLENOID
QUADRUPOLE
LENS
FARADAY CUP
0 20 40 60
SCALE: CM

7

Figure 2 Breit-Rabi diagram for deuterium showing the splitting of the $2S_{1/2}$ and $2P_{1/2}$ excited states as a function of B-field strength. M_J is the electron spin projection and M_I is the nuclear spin projection. Not drawn to scale.

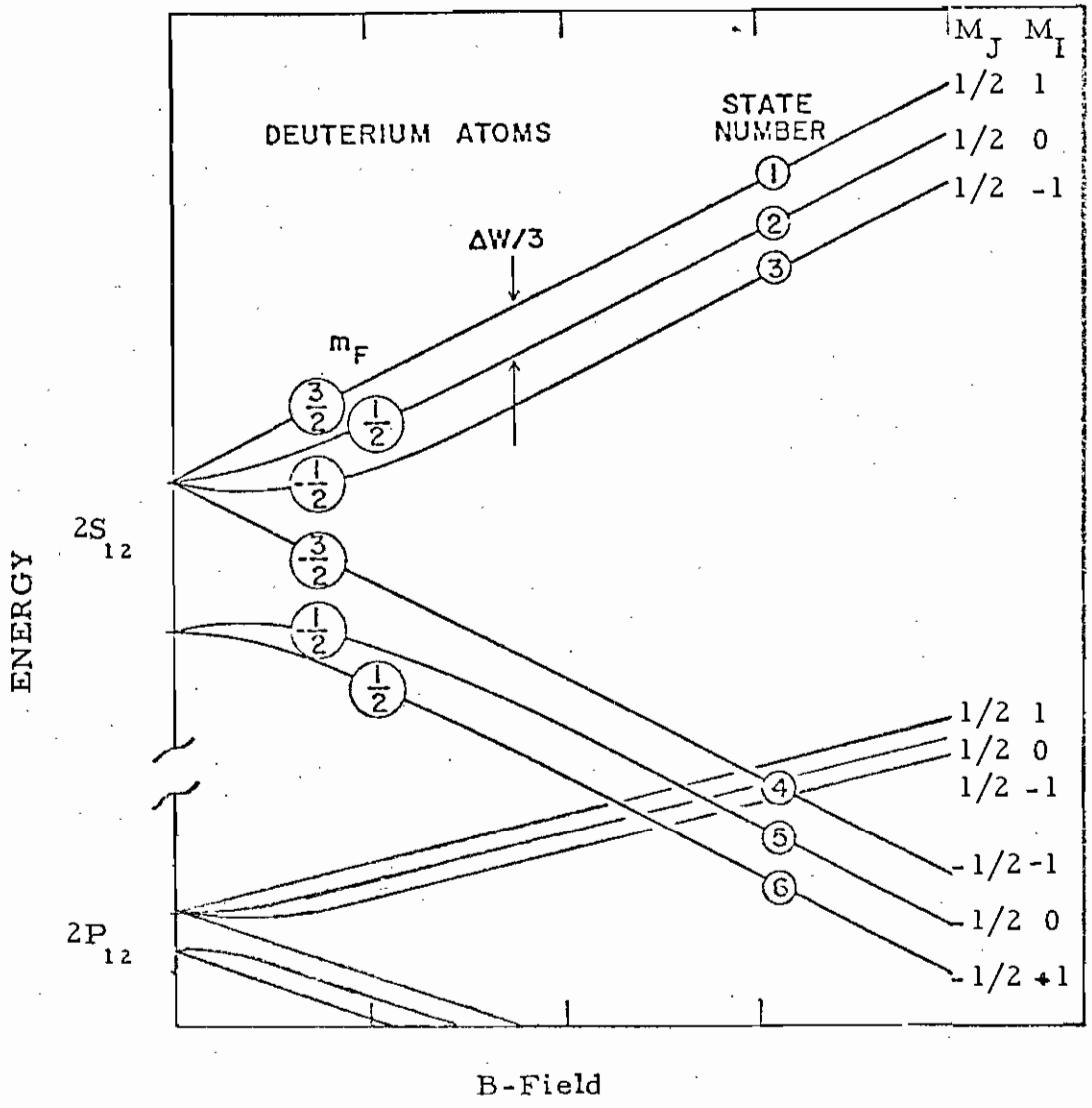
DEUTERIUM ATOMS
STATE NUMBER
M_J M_I
1/2 1
1/2 0
1/2 -1
ΔW/3
m_F
3/2
1/2
-1/2
-3/2
1/2
-1/2
1/2
$2S_{12}$
$2P_{12}$
1/2 1
1/2 0
1/2 -1
-1/2 -1
1/2 0
-1/2 +1
1
2
3
4
5
6
ENERGY
B-Field

9

Figure 3. Plot of beam current through the spin filter versus B-field with the RF power turned on. The flat background current is basically unpolarized. The three peaks represent the selection of the three substates of the $2S_{1/2}$ level with $M_J = 1/2$ (labeled as states 1, 2 and 3 in Figure 2).

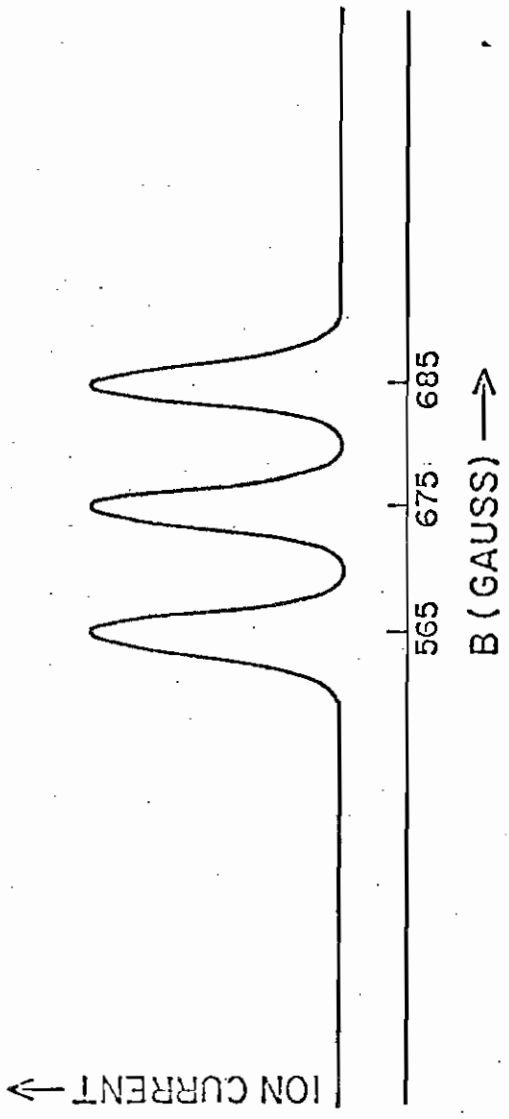
ION CURRENT
565
675
685
B (GAUSS)

way to cause transitions among selected hyperfine levels and quench certain nuclear spin projections. When the frequency of the RF E-field matches the energy difference between the two states with the same M_I, the transmission of this state through the spin filter is sharply enhanced while other components are quenched (47). In practice, the RF frequency is set at 1609 MHz and the B-field is varied to select the state transmitted. The neutral beam now passes into the argon charge exchange canal where the 2S metastable state atoms are preferentially changed to negative ions. This is due to the larger cross section for negative ion production for the 2S state than for the 1S state. This beam, now polarized, is accelerated in the usual way. There are spin precession solenoids in the source which can be used to rotate the spin axis of the deuterons to any desired direction in space. The orientation of the target chamber in the present work made this procedure unnecessary(see section II. A. 2).

During these experiments, the source developed beams of about 65-80% tensor polarization with beam currents on target of between 10 and 40 nA., averaging about 20 nA. These conditions resulted in a γ-ray detector counting rate of about 12K-15K counts/sec. for each NaI detector. Beam polarization on target was monitored at half hour intervals with the quench ratio method(47). These quench ratios were averaged over the entire measurement to determine the average polarization of the beam during the course of the experiment.

2)Accelerator

The polarized deuteron beam was accelerated to an energy of $E_d = 4.72$ MeV with the TUNL Model FN Tandem van de Graaff accelerator. The beam was momentum analyzed in a magnet system consisting of two 90° magnets with the

accelerator control slits in between. The beam then passed through a third magnet designed to divert the beam into any one of several target ports. The target chamber for this experiment was placed on the 0° port of this magnet so that the beam entering the target chamber was oriented parallel to the beam in the ion source spin filter. This meant that the quantization axis of the beam on target was the same as the B-field in the spin filter, and no reorientation of the deuteron's spin axis was necessary. Data was taken for two differing beam polarizations. For the ^{33}S measurement and one of the ^{35}S measurements data at the differing beam polarizations were normalized to the integrated beam current. For the last two measurements of ^{35}S a system was developed that allowed the on-line computer to control the ion source. The computer sensed the beam current and switched the beam polarization and regular and frequent intervals to automatically normalize the data.

3) Target Chamber

The γ-ray and particle detector arrangement are shown schematically in Figure 4. The γ-ray detectors are arranged around the chamber in a horizontal plane using three of the four quadrants on both sides of the chamber. This arrangement allowed placing the detectors within 3 cm of the chamber wall, and 10 cm from the target. The annular particle detector was mounted in a collimator assembly which was fitted into the beam pipe. This assembly also contained an insulated collimator from which beam current readings could be taken, a plastic snout to suppress particles scattered from the chamber walls, and a 25 μm Mylar foil shielding the detector to suppress α particles. The

Figure 4. Schematic diagram of the target chamber assembly. The γ-ray detectors are arranged in a horizontal plane. The annular surface barrier detector is mounted in a collimator assembly not shown.

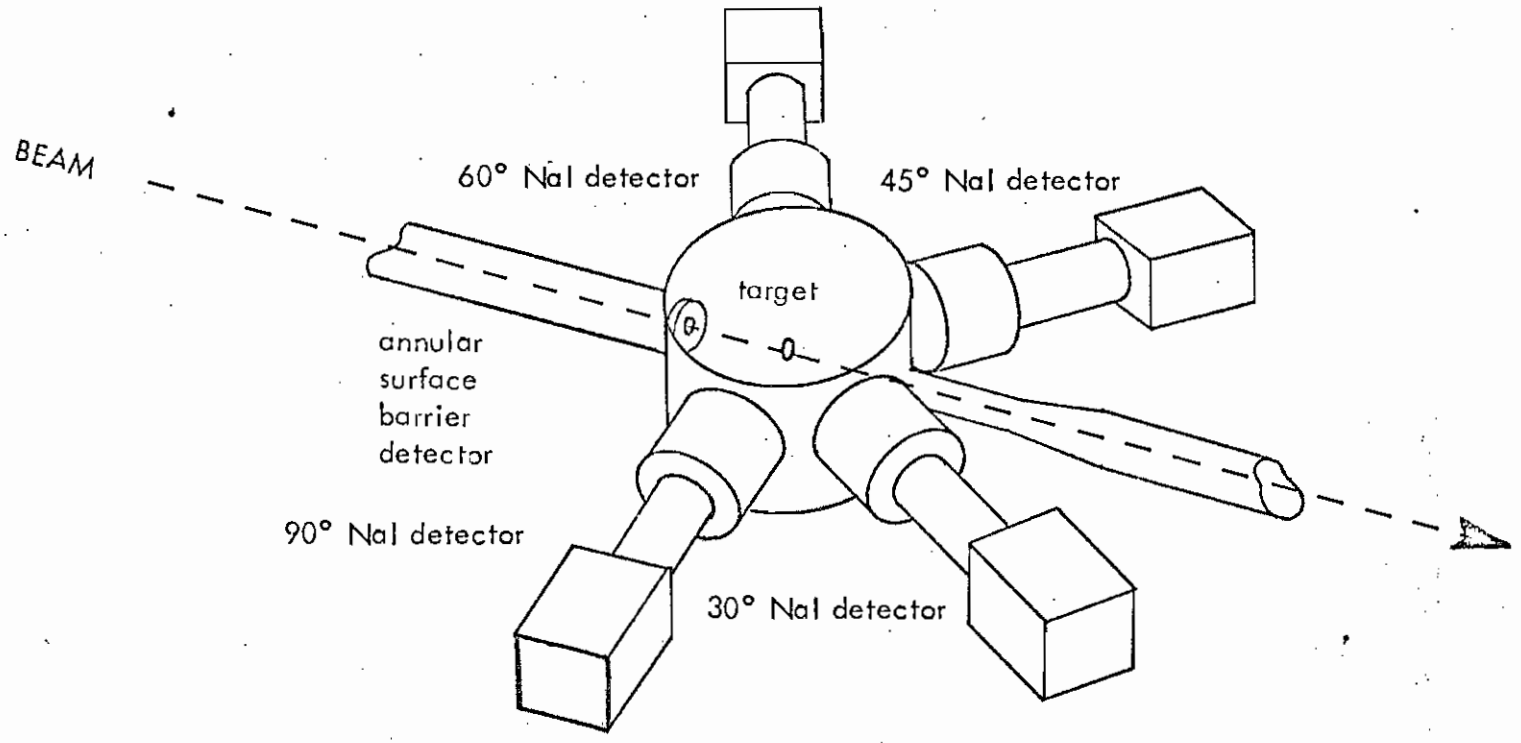

ANGULAR CORRELATION EXPERIMENTAL APPARATUS

beam was initially tuned to obtain a target current to collimator current ratio of greater than 20 : 1. The collimator was grounded during actual measurements to avoid noise problems in the particle detector system.

4) Detectors

The γ-ray detectors used in this experiment were 7.6 x 7.6 cm NaI(Tl) scintillation crystals mounted on RCA 8575 phototubes. These were integral units having a γ-ray energy resolution of about 8% for the 662 keV Cs γ-ray. The phototubes were biased at 1500 volts to allow large enough amplitude fast timing signals while avoiding tube current loading problems that would adversely affect the energy resolution. The final output of the tube was pre-amplified in a preamplifier built into the tube base assembly and then sent to the main amplifier. The fast timing signal was taken off of the anode through a capacitor and sent directly to the fast electronics.

Protons were detected with an annular surface barrier detector of 2 mm depletion depth with average particle resolution of about 40-50 keV for 6-8 MeV protons. This detector was mounted in the collimator assembly described previously, and subtended an angle at the target of between 173° and 177°. Typical particle spectra obtained with this detector are shown in Figures 6 and 13.

5) Electronics

A schematic block diagram of the electronic circuitry is shown in Figure 5. Measurements were made using a particle-γ-ray coincidence technique(48). Signals representing γ-ray energy, coincident proton energy, and time difference

Figure 5. Schematic block diagram of the electronics circuitry. A key to the nomenclature is given below.

AMP:	Linear Amplifier
CFTD:	Constant Fraction Timing Discriminator
COIN:	Overlap Coincidence
DUD:	Dual Updating Discriminator
GDG:	Gate and Delay Generator
LGS:	Linear Gated Stretcher
PG:	Pileup Gate
PRE:	Preamplifier
SUM AMP:	Summing Amplifier
TAC:	Time Analyzer
TFA:	Timing Filter Amplifier
TPO:	Time Pickoff
TSCA:	Timing Single Channel Analyzer
UC:	Universal Coincidence

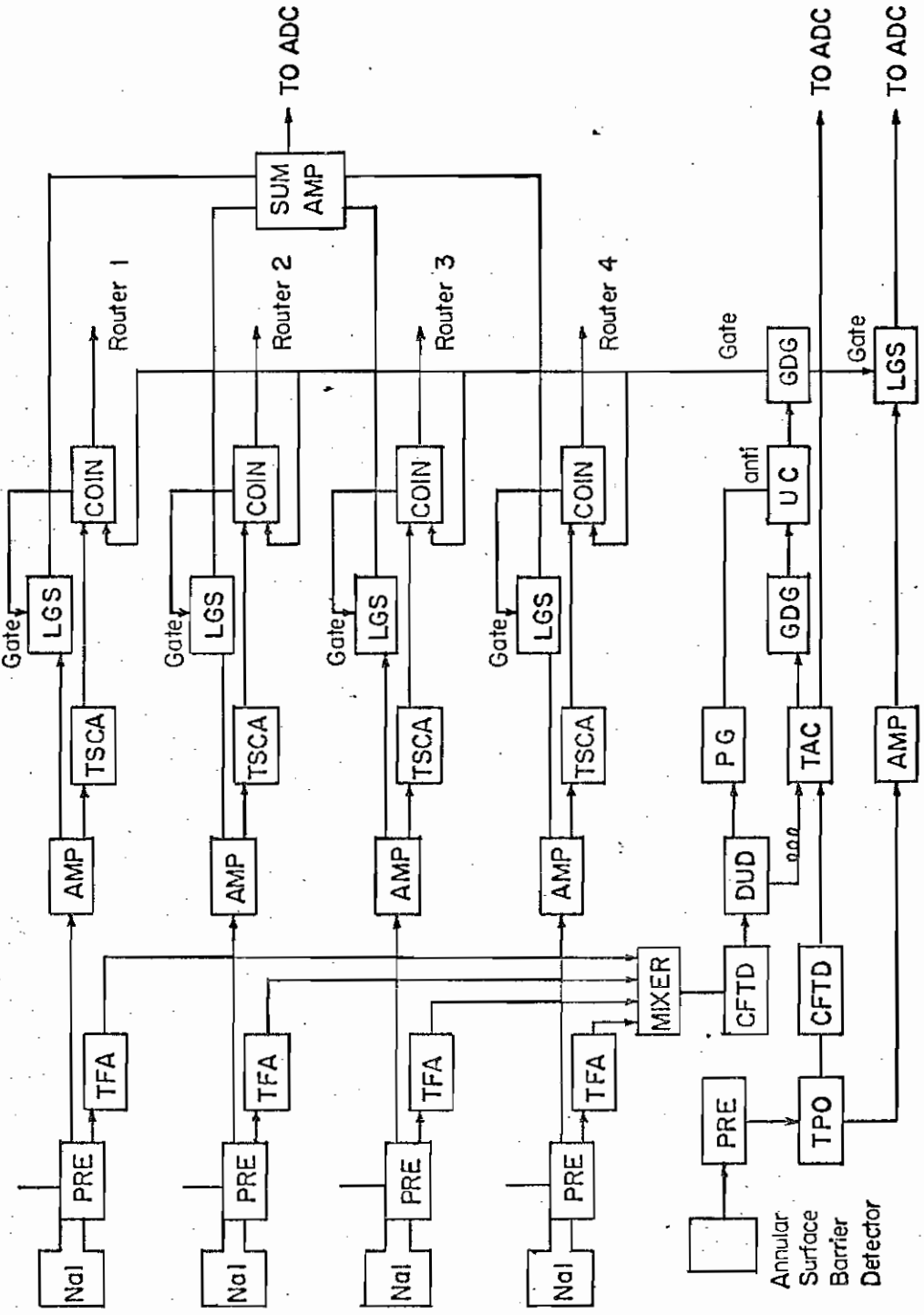
NaI
PRE
TFA
AMP
TSCA
LGS
Gate
COIN
Router 1
Router 2
Router 3
Router 4
SUM AMP
TO ADC
MIXER
CFTD
DUD
PG
anti
UC
GDG
TAC
TPO
PRE
Annular Surface Barrier Detector

between the γ-ray and particle event were generated in the electronics and sent to the computer simultaneously where they were stored event-by-event on magnetic tape for subsequent off-line analysis. As can be seen in Figure 5, each detector generated a slow linear signal and a fast (negative) timing signal. The fast signals after shaping and amplification were sent to a time to amplitude converter (TAC) which generated an output for every valid coincidence event. The γ-ray fast signals were also sent to a pileup gate (PG) which generated a logic output for every piled up event. This output blocked the output of the TAC so pileup events did not reach the computer. The TAC output, now representing all real coincident events, was used to gate open the linear gated stretchers (LGS) to allow the particle and γ-ray linear signals to reach the analog-to-digital converters (ADC).

Each linear signal circuit consisted of a preamplifier, amplifier, and linear gated stretcher to process the signal for the ADC. In addition, the bipolar γ-ray amplifier outputs were sent to timing single channel analyzers (TSCA) and then to overlap coincidence units (COIN). The output of the coincidence units served both to open the γ-ray linear gate and to provide a routing signal to the computer interface.

6) Interface and Computer

The computer interface consisted of the analog-to-digital converters, the router, and associated control electronics. Gamma-ray energy, proton energy, coincidence time, and monitor proton energy signals were sent to separate ADC's. The first three of these arrived at the ADC's simultaneously and were

processed together. The on-line computer program (48) read the output of the ADC's, wrote the information on magnetic tape, and recycled to await the next coincidence event.

The singles monitor proton spectrum was handled asynchronously by the computer. This singles spectrum was stored in memory during the course of a measurement. At the end of the measurement it was written on magnetic tape in binary format and used for normalization purposes during later analysis.

The outputs from the γ-ray timing single channel analyzers were sent to the router which sent a 3 bit word to the computer telling it which detector originated the event. The router also detected pile-up events defined as those with two or more simultaneous inputs at the router. These events were discarded by the computer and not written on tape. All events which had valid signals in three ADC's were stored on magnetic tape.

B. Target Preparation

The targets used in this experiment consisted of elemental sulfur of about 100 $\mu g/cm^2$ thickness, sandwiched between thin layers of gold. Targets for the $^{32}S(\vec{d},p\gamma)^{33}S$ reaction were natural sulfur. Targets for the $^{34}S(\vec{d},p\gamma)^{35}S$ experiment were made with isotopically enriched (90%) ^{34}S. This method made a target that was both thin (good particle resolution) and efficient (high percentage sulfur by weight).

These targets were developed after much experimentation. The preliminary measurements were made using targets of CdS evaporated onto tantalum

backing foils. These were fairly satisfactory but were only 22% sulfur by weight. Yields were low relative to target thickness. It was decided that since the beam currents would be small, it would be worthwhile having an elemental sulfur target.

The problem was that elemental sulfur would sublime at a rapid rate in a vacuum, especially when bombarded by a beam. The solution devised for this problem was to sandwich the sulfur between covering layers of some non-porous material. Gold was chosen because of its low melting point and high tensile strength. Gold also had a relatively high Z (79) which minimally degraded the particle resolution. The low evapporation temperature proved to be very important as the sulfur would sublime while the gold overcoating was being deposited if great care wasn't taken. After several approaches, the following procedure was finally adopted:

a) Clean microscope slides were placed in an evacuated bell jar over a tungsten boat in which was placed a small (1 mm) bead of gold and a small grain of cesium iodide. The boat was electrically heated, evaporating the cesium iodide first, which coated the slides with a water soluble release agent. The gold evaporated at a higher temperature and was depasited to a thickness of about 50 $\mu g/cm^2$.

b) The gold coated slides were then removed from the evaporater. Sulfur was deppsited by holding the slides over a small aluminum crucible into which sulfur was placed and which was heated by a hot plate. This crucible was heated just hot enough to melt the sulfur grains. A few grains were added at a time, and the slides were

held close over the crucible while the sulfur fumed. Keeping the slide near room temperature proved to be critical. The trick was to avoid allowing the slide to become so hot that the sulfur already deposited was re-evaporated. (an attempt to avoid high temperature by cooling the slides to about 50°F proved a failure---condensation prevented sulfur from depositing at all.) This temperature balance proved to be the touchiest part of the entire operation.

c) The slides were replaced in the evaporater as rapidly as possible and a gold overcoating was evaporated on top. The faster this step could be accomplished, the thicker the targets were.

d) The slides were taken from the evaporater and the gold-sulfur-gold layered target was floated off on water, picked up on a target ring and allowed to dry. This part of the procedure was standard. The targets proved no more fragile than 20 $\mu g/cm^2$ carbon foils.

Several natural sulfur targets were made in this way, and two good ^{34}S targets were made with thicknesses of about 80-100 $\mu g/cm^2$. About 4 mg of ^{34}S was used to prepare these two targets. This system made more efficient use of isotope than would a procedure that used the evaporater to deposit the sulfur, where a large fraction of isotope would be deposited on the walls of the evaporater.

The targets were tested for evaporative losses at beam currents of between 50-100 nA (unpolarized deuterons) and no decrease in yield was detected over 24 hours running time. Polarized beam currents on target were never greater than 40 nA.

C. Analysis

1) Angular correlation theory

The idea of using symmetries in a reacting system to simplify the interpretation of an angular correlation measurement was first pointed out by Biedenharn, et. al.(35) and first applied experimentally by Warburton and Rose (36). The method of axial symmetry is due to Newton (37), and the explicit form used here was derived by Litherland and Ferguson (41). The measurement and analysis of angular correlations has been discussed at great length by many authors (35-44) and the literature contains complete derivations of the formalisms for experiments involving both unpolarized and polarized projectiles. The basic problem is one of measuring the characteristics of the γ-ray radiation emitted in the decay of an excited state of definite spin and parity, and relating these to the properties of the nuclear wave functions. Aside from an absolute intensity and energy, the γ-ray angular distribution in space and polarization can be measured. A discussion of γ-ray polarization won't be attempted here. It is irrelevant to the present experiment and has been discussed in depth in the literature.

To understand the use of angular correlations, consider the reaction $A(a,b)B(\gamma)C$, where B represents an excited state of definite spin and parity of the residual nucleus that decays by γ-ray emission. (A is the target nucleus and a is the beam projectile.) The amplitude for transitions between definite magnetic substates (M,m) with γ-ray emission in the $\vec{k}$ direction and with polarization $\vec{e}$ is in general proportional to (44)

$$\sum_{M_B} \langle J_C M_C | H_e(\vec{k},\vec{e}) | J_B M_B \rangle \langle \vec{k}_b\ J_B M_B s_b m_b \mid T \mid \vec{k}_a, J_A M_A s_a m_a \rangle$$

where J is the spin of the nuclear state, s is the spin of the particle, and M and m are the corresponding z-components. The second factor in this expression is the transition amplitude for the reaction A(a,b)B. The first factor is the amplitude for emission of a γ-ray of momentum $\vec{k}$ and polarization $\vec{e}$. With this nomenclature the differential cross-section for the A(a,b)B reaction is proportional to (ignoring phase and normalization factors)

$$d\sigma/d\omega_b \approx ((2J_A+1)(2s_a+1))^{-1} \langle \vec{k}_b\ J_B M_B s_b m_b \mid T \mid \vec{k}_a\ J_A M_A s_a m_a \rangle^2$$

The double differential cross-section for emission of b along $\vec{k}_b$ and γ along $\vec{k}$ is proportional to

$$d^2\sigma/d\omega_b d\omega_\gamma \approx W(\theta_\gamma,\varphi_\gamma)\ d\sigma/d\omega_b$$

where

$$W(\theta_\gamma,\varphi_\gamma) = \sum_{kq} A_{kq}(\vec{k}_a,\vec{k}_b)\ C_{kq}(\theta_\gamma,\varphi_\gamma)$$

C is a spherical harmonic proportional to Y_k^q and A_{kq} is a correlation coefficient composed of two parts,

$$A_{kq}(\vec{k}_a,\vec{k}_b) = B_{kq}(J_B)R_k(\gamma)$$

The B_{kq} are complex numbers that require specific reaction mechanism information for their description. $R_k(\gamma)$ depends on only the parameters of the γ-ray transition.

$$R_k(\gamma) = \sum_{LL'} g_L g_{L'} R_k(LL'J_B J_C)$$

where L and L' are the multipoles of the γ-ray transition and $R_k(LL'J_B J_C)$ are real numbers defined in (40). The g_L and $g_{L'}$ are the multipole amplitudes

$$g_L = \frac{\langle J_B \| T_L^{\pi} \| J_C \rangle / (2L+1)^{1/2}}{\left(\sum_{L'} \langle J_B \| T_L^{\pi} \| J_C \rangle^2 / (2L'+1)\right)^{1/2}}$$

where T_L^{π} are electromagnetic interaction tensors defined in (40). The mixing ratio measured in the present experiment is defined as

$$\delta = g_{L+1}/g_L$$

$\Sigma g_L^2 = 1$ so that g_L^2 is the fraction of the decay proceeding by 2^L pole radiation. Note that this definition is identical to that of Poletti and Warburton (66) who define the mixing ratio as

$$x = \langle b \| L+1 \| a \rangle / \langle b \| L \| a \rangle$$

since, as shown in (43), the $(2L+1)^{1/2}$ factors have been absorbed into the L operators in ref. (66) notation. (see (43), page 319) In the general case,

the determination of the $B_{kq}(J_B)$ coefficients requires specific assumptions about the reaction mechanism. Information on the alignment of the residual nucleus (relative population of the possible M_B substates) is contained in the B_{kq}'s. Some simplification is necessary to remove this dependence. This simplification involves the co-linear geometry analyzed in detail by Litherland and Ferguson (38). The outgoing light reaction product b is detected along the beam axis so that $\vec{k}_a$ and $\vec{k}_b$ are parallel (or antiparallel). This condition implies that a, b, and B can have no projection of orbital angular momentum ℓ along the quantization (beam) axis, and

$$|M_B| \leq M_A + m_a + m_b$$

For an $(\alpha, n\gamma)$ reaction, for example, on an even A target, this implies that $|M_B| \leq 1/2$, which means that the residual nucleus is aligned in all cases except when $J_B = 1/2$. This means that the population parameters of the residual nucleus are known, and that the correlation function W is no longer a function of the coefficients B_{kq}. For the $(d, p\gamma)$ reaction on an even A target, $|M_B| \leq 3/2$, since the deuteron has spin 1. Consequently states in the residual nucleus with $J = 1/2$ or $3/2$ are not aligned. The correlation function is then a sum of terms with differing M_B and the determination of mixing ratios is much more difficult (usually impossible). The way around this problem is to somehow restrict m_a or m_b. For a $(d, p\gamma)$ reaction this means restricting m_a to zero.

As shown in section II. A. the polarized source generates a beam of protons or deuterons with unequal populations of the available magnetic substates. For deuterons, $m_a = 1, 0$ or -1 relative to some quantization axis, in this case the axis of the B-field in the spin filter. A complete description of the beam polarization referred to an arbitrary set of coordinate axes would require the use of the polarization tensor (see appendix). Relative to the quantization axis used here, however, it can be seen that two numbers suffice to describe the relative populations of the three substates. The Madison Convention (45) proposed that the two quantities "vector polarization" and "tensor polarization", p_z and p_{zz}, be defined as follows:

$$p_z = N_1 - N_{-1} \qquad p_{zz} = N_1 + N_{-1} - 2N_0$$

where N_1, N_0, and N_{-1} are the populations of the $m_b = 1, 0, -1$ substates respectively, and $N_1 + N_0 + N_{-1} = 1$. The vector polarization p_z varies between 1 and -1, and the tensor polarization can vary between 1 and -2. Both are zero for an unpolarized beam ($N_1 = N_0 = N_{-1} = 1/3$). Qualitatively, p_z describes the difference between the population of the parallel and anti-parallel spin projections, and p_{zz} describes the relative population of the $m_a = 0$ projection. P_{zz} is the quantity of interest in the present experiment. If $p_{zz} = -2$, the deuterons all have $m_a = 0$ and,

$$|M_B| \leq 1/2$$

If a beam with $p_{zz} = -2$ could be achieved in practice, a single correlation measurement could be made and analyzed in the same way as an $(\alpha, n\gamma)$ angular correlation. Perfect beam polarization is not attainable in practice and any single measured angular correlation always has some component contributed by the $M_B = \pm 3/2$ substate of the residual nucleus B. There exists a linear combination of two correlations however, of arbitrary but different polarizations, that does not have a contributing $M_B = \pm 3/2$ component. As described below, this combination can be analyzed assuming $M_B = \pm 1/2$ and is referred to as $W(\theta)$ in all the experimental diagrams to follow.

To show that a combination of two correlation measurements of differing beam polarizations can be combined to yield a correlation independent of the populations of the M_B substates, consider the following argument, which closely follows the treatment given in (42).

The B_{kq} describe the orientation of the residual nucleus caused by the reaction A(a,b)B.

$$B_{kq} = \Sigma\, C^{q}_{kk_1}(s_a)\, p(s_a)$$

where $p(s_a)$ is a matrix describing the beam polarization, and the $C^{q}_{kk_1}(s_a)$ now contain the reaction information. Now average the correlation function in azimuth to account for the co-linear geometry,

$$\bar{W}(\theta) = \frac{1}{2\pi} \int_0^{2\pi} W(\theta, \varphi)\, d\varphi$$

For an unpolarized deuteron beam,

$$\bar{W}_u(\theta) = \frac{1}{\sqrt{3}} \sum_k C^o_{ko}(1)\ R_k P_k(\cos\theta)$$

For a polarized deuteron beam,

$$\bar{W}(\theta) = \bar{W}_u(\theta) + \frac{1}{\sqrt{6}}\, p_{zz} \sum C^o_{k2}\ R_k P_k(\cos\theta)$$

McCullen and Seyler show that (42)

$$C^o_{k2} - \frac{1}{\sqrt{2}}\, C^o_{ko} = \frac{1}{\sqrt{6}} (C\ -\tfrac{1}{2}, C\ \tfrac{1}{2} \mid k0)\ U_{1\frac{1}{2}}$$

Where U is a factor independent of k and $(C\ -\frac{1}{2}, C\ \frac{1}{2} \mid k0)$ is a Clebsch-Gordon coefficient. The combination,

$$W(\theta) = \bar{W}(\theta) - (1+\tfrac{1}{2}\, p_{zz})\, \bar{W}(\theta) = p_{zz} U_{1\frac{1}{2}} \sum (C\ -\tfrac{1}{2}, C\ \tfrac{1}{2} \mid k0)\ R_k P_k(\cos\theta)$$

is independent of the reaction mechanism except through an overall normalization factor.

For the case where two measurements at differing non-zero beam polarizations α and β are made, the equation can be put in the form (68),

$$W(\theta) = \bar{W}_\alpha - \left(\frac{2+p^\alpha_{zz}}{2+p^\beta_{zz}}\right) \bar{W}_\beta$$

It is evident that optimum results are obtained when $p_{zz}^{\alpha'}$ and p_{zz}^{β} differ by as much as possible, so that the term multiplying $\overline{W}_{\beta}$ is small.

2) Data Reduction

The data written on magnetic tape during the measurements was analyzed according to the following routine:

a) The magnetic tape was first read in such a way that all coincident particle events were stored in the computer and the channel numbers of all peaks of interest were recorded.

b) The tape was read a 2nd time--- all time events which also had a particle event within a preselected window in the particle spectrum were read into the computer. This time spectrum consisted of a single peak representing true coincidence events and a random coincidence background.

c) The tape was read a 3rd time--- all γ-ray events that corresponded to time events and particle events falling within the specified windows are read into the computer. This γ-ray spectrum represented the γ-rays in true coincidence with the proton group of interest in the residual nucleus. A subtractive correction was made for random coincidences by subtracting any γ-ray event whose time event fell within a time interval in the background region of the time spectrum. This random interval was of the same size as the true coincidence time window.

d) Photopeak areas and centroids (first moments) were extracted by fitting a polynomial to the area around the peak and then calculating the area and centroid of the peak after subtracting the background. From these areas an angular correlation was obtained which gave the yield as a function of γ-ray detector angle.

3) Fitting Procedure

The angular correlations for the two different values of the beam polarization were combined as discribed in section II.C.1 to yield the angular correlation $W(\theta)$ which is independent of the $M_B = \pm 3/2$ substates of the residual nucleus. The theoretical $W(\theta)$,

$$W(\theta) = \sum_{\substack{i \\ \text{even}}} A_i Q_i P_i(\cos\theta)$$

were fitted directly to the data by the computer code M2 (65) in a way similar to that of Poletti and Warburton (66), and optimum values of the A_i coefficients were calculated. A notation change has been made here to conform to the notation normally used in this laboratory (68), where A_i are the correlation coefficients and the Q_i are attenuation coefficients designed to account for the finite size of the NaI detectors. The Q_i's were calculated by the code M2. The program calculates the values of the A_i coefficients that minimize X^2.

$$X^2 = \frac{1}{n} \sum_i \left(\frac{Y(\theta_i) - W(\theta_i)}{\Delta Y(\theta_i)} \right)^2$$

for a series of values of arctan δ ranging from $-90°$ to $+90°$ (corresponding to varying δ from $-\infty$ to $+\infty$). The X^2 is a measure of the "goodness of fit" or agreement between the two functions Y and W. It is defined in such a way that its magnitude is related to the quality of the data compared to the theoretical prediction. For "perfect" data, for instance, where $Y(\theta_i) = W(\theta_i)$ for all θ_i, X^2 would equal zero. In general, the smaller the minimum value of X^2, the better the agreement between theory and experiment, and the better the overall quality of the data.

The program output consisted of the value of X^2 for each value of δ in the stepping procedure, the best overall fitted value of δ and the corresponding (minimum) value of X^2, the statistical errors for the solution to the mixing ratio, the values of the A_i coefficients, and the theoretical fit to the data. The sign convention for δ is that of Rose and Brink (43). The errors in the multipole mixing ratio were calculated by the code M2 in accordance with the iterative procedure discussed by Smith (67).

Chapter III

RESULTS

Angular correlations and X^2 fits for ^{33}S and ^{35}S are shown in Figures 8 - 12 and Figures 15 - 20, respectively. A summary of experimental results for ^{33}S is compiled in Table 1 and for ^{35}S in Table 2. In Table 2, the 5th and 6th columns contain multipole mixing ratio results for the three separate measurements. The 7th column labeled "average δ" contains weighted averages of the individual measurements. The calculated matrix elements B(L) and B(L+1) shown are calculated using the average value of δ. Excitation energies, J^{π}, mean lives, branching ratios, and any previously measured values of δ for ^{33}S are taken from (5) and (23) unless otherwise noted. Corresponding experimental information for ^{35}S is taken from (28) unless otherwise noted. Energy level diagrams for ^{33}S and ^{35}S are shown in Figures 7 and 14, respectively. Figures 6 and 13 show coincident proton spectra for these two nuclei. Peaks of interest are identified by their excitation energies in keV.

Note that in all figures displaying angular correlation results, the data points drawn as triangles and squares are actual measured correlations. The circular points labeled W(θ) are the combination of the two measured correlations (see II.C.1) which is analyzed, and is not a separate measurement. Errors bars shown represent statistical errors. The curves plotted through the data are the fitted theoretical correlations for the best X^2 fits.

Page 33 is not included in the thesis book.

Figure 6. Coincident proton spectrum for the $^{32}S(\vec{d},p\gamma)^{33}S$ reaction at $E_d = 4.72$ MeV. Numbers labeling the peaks are the excitation energies of the levels in ^{33}S in keV.

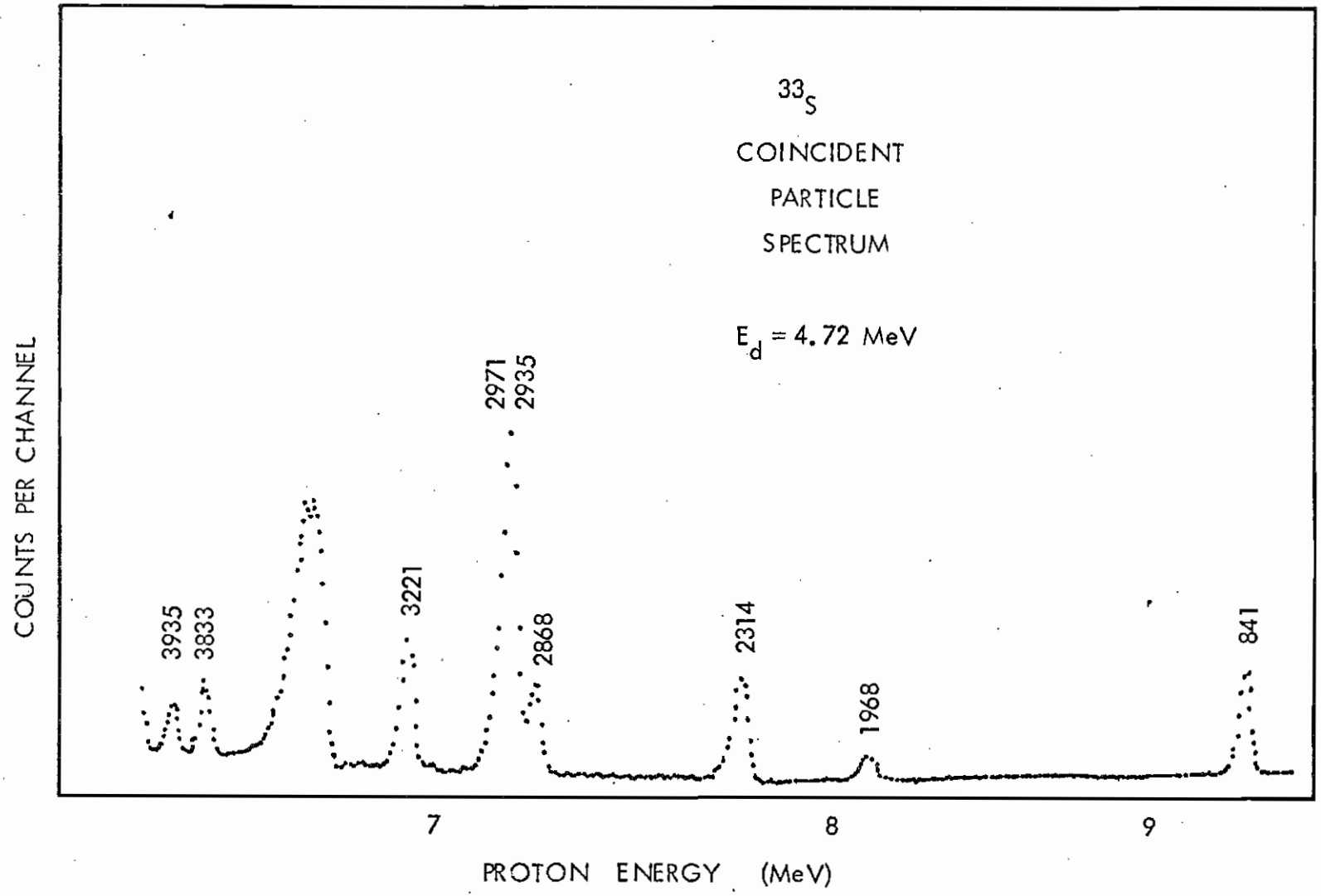
^{33}S
COINCIDENT
PARTICLE
SPECTRUM
E_d = 4.72 MeV
COUNTS PER CHANNEL
3935
3833
3221
2971
2935
2868
2314
1968
841
7
8
9
PROTON ENERGY (MeV)

Figure 7. Energy level diagram for ^{33}S. E_x, J^π, and τ_m are taken from (5).

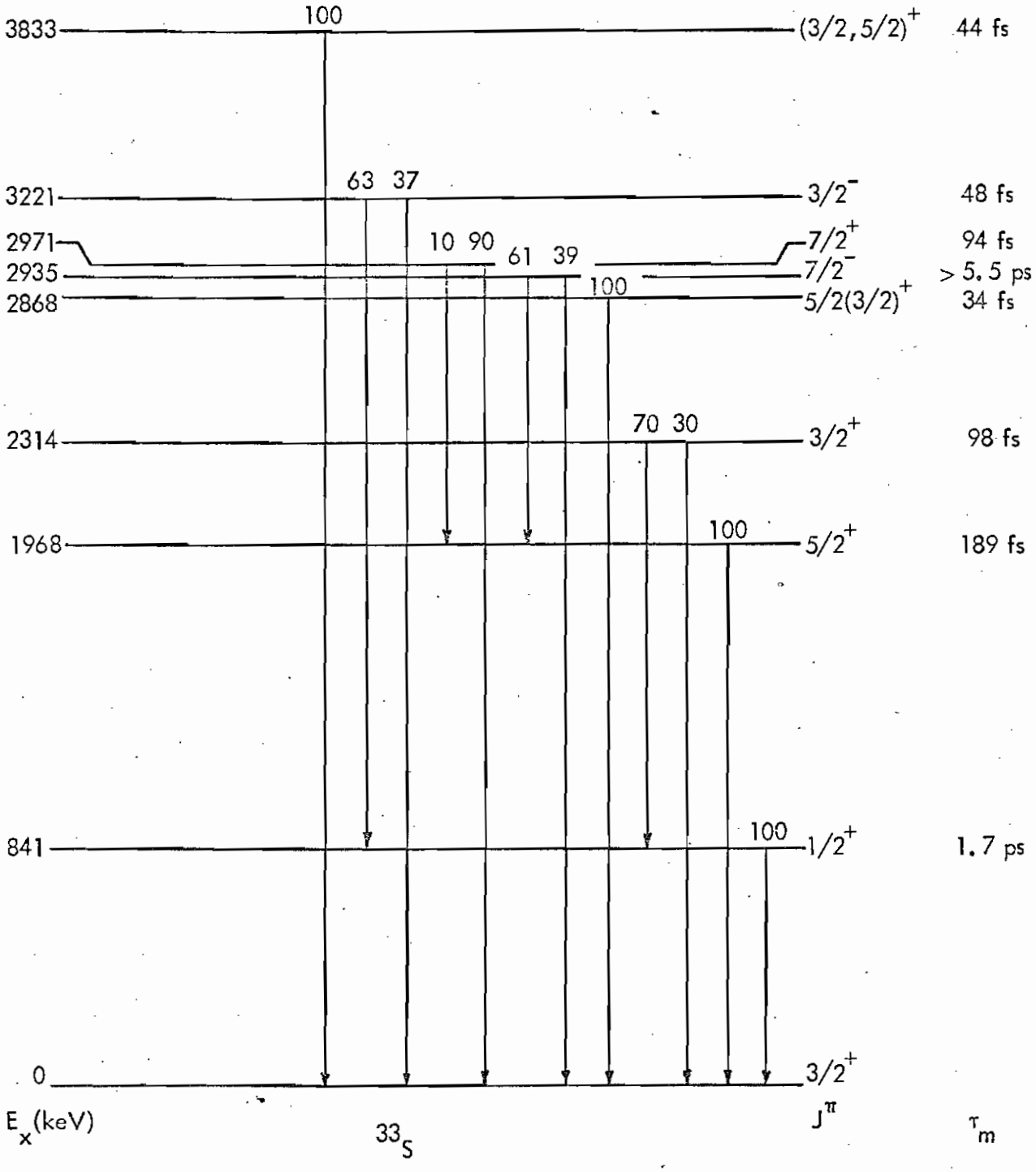
3833
100
(3/2,5/2)+
44 fs
3221
63 37
3/2−
48 fs
2971
10 90
61 39
7/2+
94 fs
2935
7/2−
> 5.5 ps
2868
100
5/2(3/2)+
34 fs
2314
70 30
3/2+
98 fs
1968
100
5/2+
189 fs
841
100
1/2+
1.7 ps
0
3/2+
Ex(keV)
33S
Jπ
τm

One angular correlation measurement was made for levels in ^{33}S involving about 30 hours of accelerator running time. The array of 4 NaI detectors was used as shown in Figure 4. Three angular correlation measurements were made for ^{35}S: 2 with the 4 detector array comprising about 100 hours of running time, and 1 with the 5 detector array comprising about 60 hours of running time.

A. Results for ^{33}S

1) The 841 keV Level

The angular correlations and X^2 analyses for the first excited state are shown in Figure 8. The combined correlation $W(\theta)$, shown as circles on the plot of relative yield versus $\cos^2\theta$, is isotropic to within statistics. This is consistent with the known $J^\pi = 1/2^+$ of this level, and the graph of X^2 versus arctan δ shows that a $J = 1/2$ hypothesis yields an excellent fit to the data. (The value of X^2 for $J = 1/2$ is a constant as a function of δ and is not drawn completely across the diagram for clarity.) The confidence level percentages shown on the right in the lower half of the figure are an absolute indicator of the goodness of fit and are related to the probability that the solution obtained for the given set of parameters is the right one. (See Ref. (69) for a compilation of these probabilities.) In angular correlation studies a spin hypothesis is rigorously excluded only if the minimum value of X^2 never exceeds (i.e. X^2 never less than) the 0.1%

Figure 8. Angular correlation results for the ground state transition from the 841 keV level in ^{33}S. The lower part of the figure shows X^2 plots for J=1,3,5/2. The upper part of the figure shows the angular correlation data. Square and triangular points represent two correlations taken with differing p_{zz}. Circular data points represent the combined correlation that is fitted to the theoretical expression. The line shown is the best least-squares fit for J=1/2.

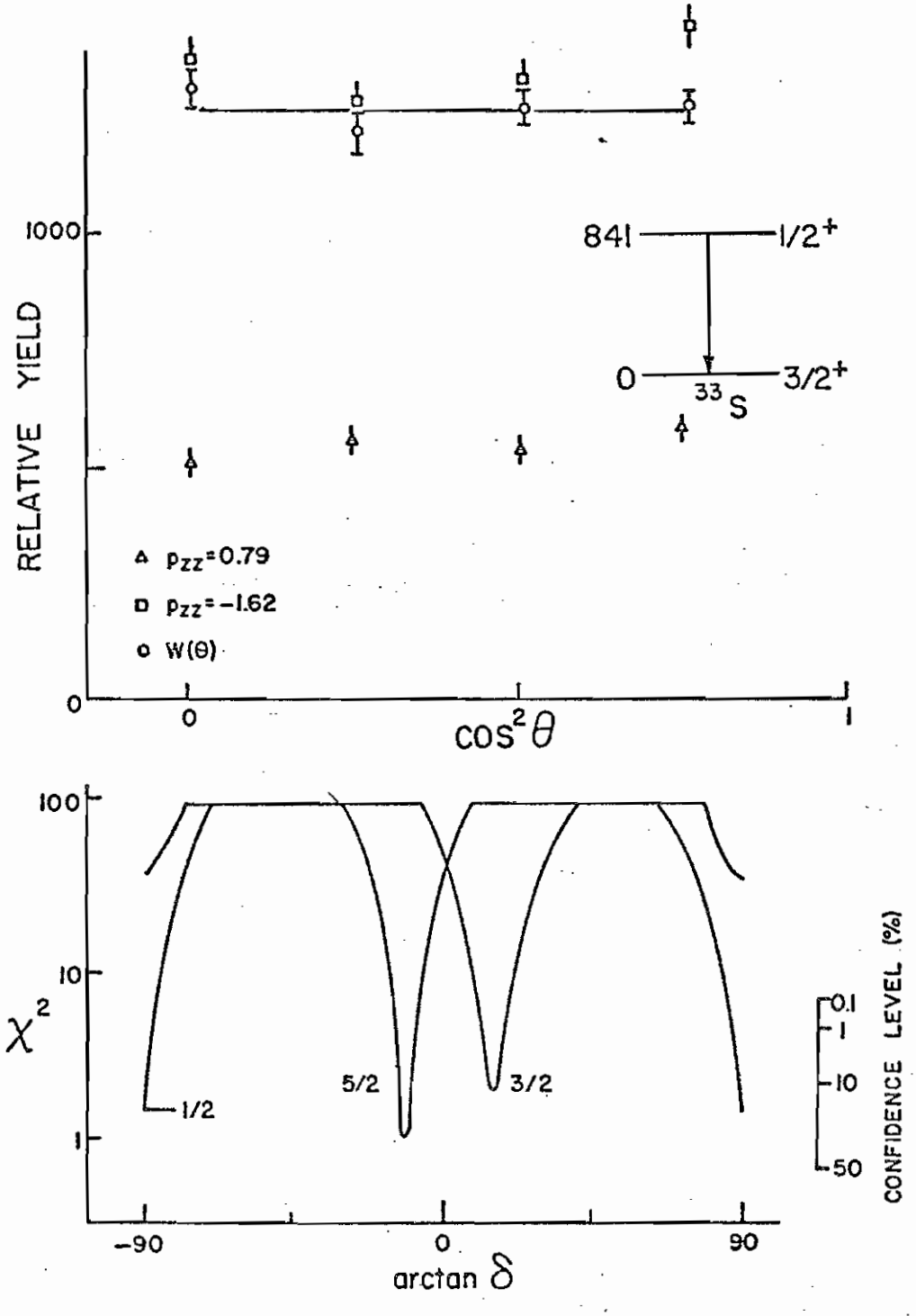
RELATIVE YIELD
1000
1
0
0
1
cos²θ
841
1/2⁺
0
3/2⁺
33 S
Δ pzz=0.79
□ pzz=-1.62
○ W(θ)
χ²
100
10
1
1/2
5/2
3/2
-90
0
90
arctan δ
CONFIDENCE LEVEL (%)
0.1
1
10
50

confidence limit for all possible values and combinations of the fit parameters. Thus for example, in the present case acceptable fits to the data also exist for spin hypotheses 3/2 and 5/2. The final spin determination had to be made by other means. In this case, the 841 keV level has $\ell_n = 0$, implying $J^\pi = 1/2^+$.

2) The 1968 keV Level

The angular correlations and X^2 analyses for J = 3/2 and 5/2 are shown in Figure 9. Of the possible values of J fitted to the data (J=1/2 through 9/2) only J=3/2 and J=5/2 spin hypotheses exceeded the 0.1% confidence limit. These two curves are shown in the lower half of the figure. Although both J's exceed the confidence limit, the J = 5/2 fit has a better absolute minimum in X^2. This fact helps confirm the known spin of this level of $J^\pi = 5/2^+$ and the value of $\delta = 0.34 \pm 0.13$ obtained for the minimum of the X^2 fit near arctan $\delta = 20^\circ$ compares favorably with the value of $\delta = 0.56 \pm 0.18$ measured by Toulemonde and Schultz (23) using the $^{30}Si(\alpha, n\gamma)^{33}S$ reaction and γ-ray angular distributions. Their measurements were made in singles using a Ge(Li) detector. Running just above the reaction threshold for the level of interest, they were able to predict the populations of the magnetic substates of the residual nucleus using a statistical model and assume that mostly s-wave (ℓ_n=0) neutrons were emitted in the reaction. This technique for limiting the substates in the residual nucleus makes the experiment similar in principle to the co-linear geometry technique employed in the present work, and the results should agree. A possible solution in the X^2 analysis corresponding to J=5/2 and δ =1.6 is ruled out by (23). This latter solution has a deeper

Figure 9. Angular correlation results for the ground state transition from the 1968 keV level in ^{33}S. The lower part of the figure shows plots of X^2 versus arctan δ for J=3,5/2. The upper part of the figure shows the angular correlation data. Square and triangular paints represent the two experimental correlations taken with differing p_{zz}. Circular data points represent the combined correlation that is fitted to the theoretical expression. The line shown is the best least-squares fit for J=5/2.

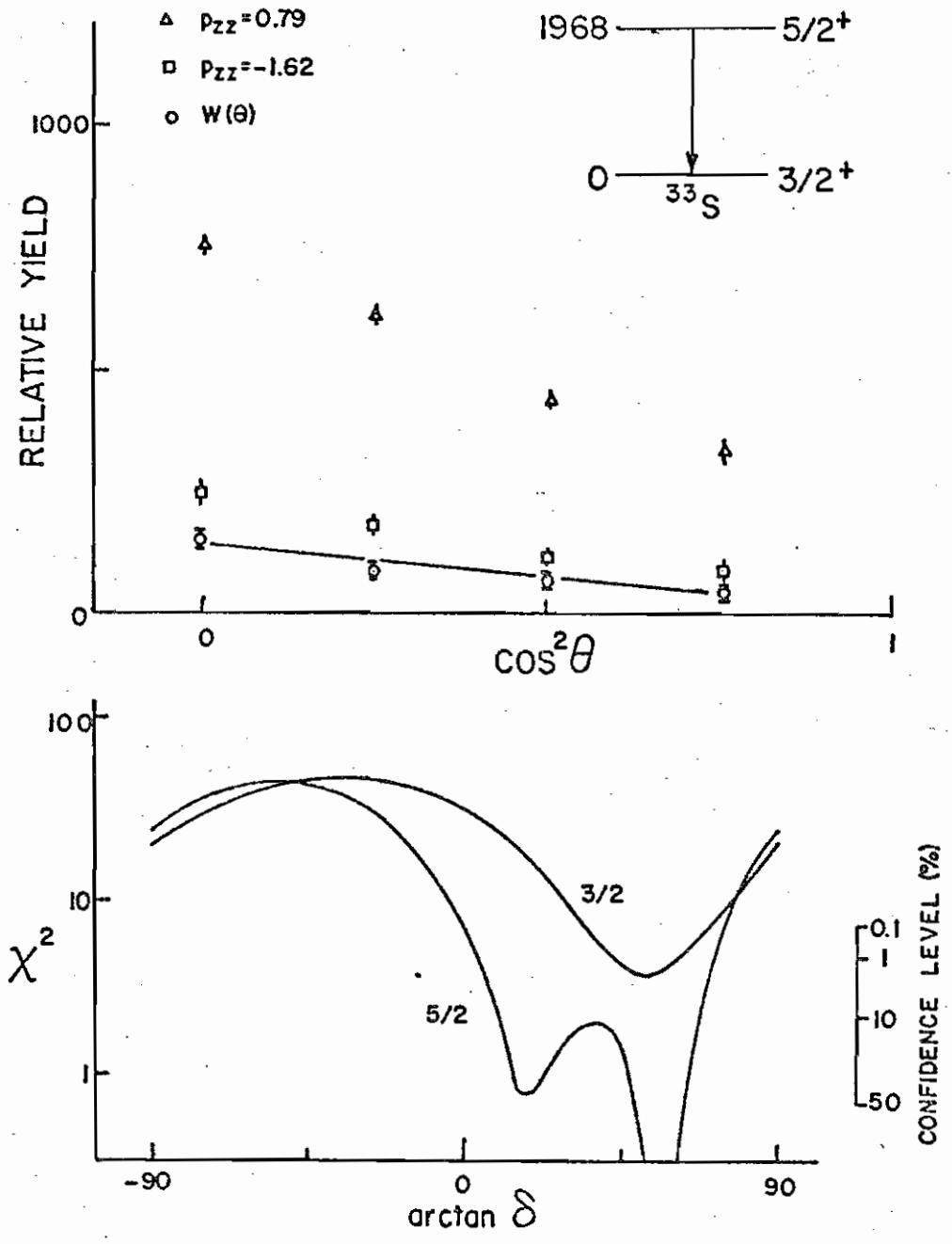
Pzz=0.79
Pzz=-1.62
W(θ)
1968
5/2+
0
3/2+
33S
RELATIVE YIELD
1000
0
0
1
cos²θ
100
10
1
χ²
3/2
5/2
-90
0
90
arctan δ
0.1
1
10
50
CONFIDENCE LEVEL (%)

X^2 minimum than the solution at 20°, but as shown by the relative confidence levels, the difference is not statistically significant. The value of δ=0.34 is taken to be the correct solution, in agreement with Ref. (23). This leads to transition strengths for the E2/M1 multipoles of 2.4 and 0.02 W.u., respectively.

3) The 2314 keV Level

The angular correlations and X^2 analyses for the ground state branch of this level are shown in Figure 10. The lower part of the figure shows plots of X^2 versus arctan δ for spin hypotheses of J=3/2 and 5/2. Fits for J=7/2 and 9/2 had X^2 minima of 18 and 20, respectively, well above the 0.1% confidence limit. Spin 1/2 was fitted for $X^2 \approx 2$. As shown, the data allows a good X^2 fit for the known spin $J = 3/2^+$. Values of the mixing ratio corresponding to the two minima in the plot are $\delta = 0.38 \pm 0.10$ and $\delta = 9^{+38}_{-4}$. These results are in excellent agreement with previous measurements of δ=0.28±0.08 or $\delta > 11.4$ by Toulemonde and Schultz (23). The values of $\delta = 0.38$ and 9 correspond to E2 transition strengths of 0.37 and 2.4 W.u., respectively. Both of these possible values are reasonable when compared to results for similar transitions in other nuclei in this mass region (64). Endt and van der Leun (64) have set an upper limit on allowable E2 strengths of 100 W.u. based on a statistical study of all available experimental evidence on nuclei in this mass region. Both solutions in the present case fall well within this range.

Figure 10. Angular correlation results for the ground state transition from the 2314 keV level in ^{33}S. The lower part of the figure shows plots of X^2 versus arctan δ for J=3,5/2. The upper part of the figure shows the angular correlation data. Square and triangular points represent the two experimental correlations taken with differing p_{zz}. Circular points represent the combined correlation that is fitted to the theoretical expression. The line shown is the best least-squares fit for J=3/2.

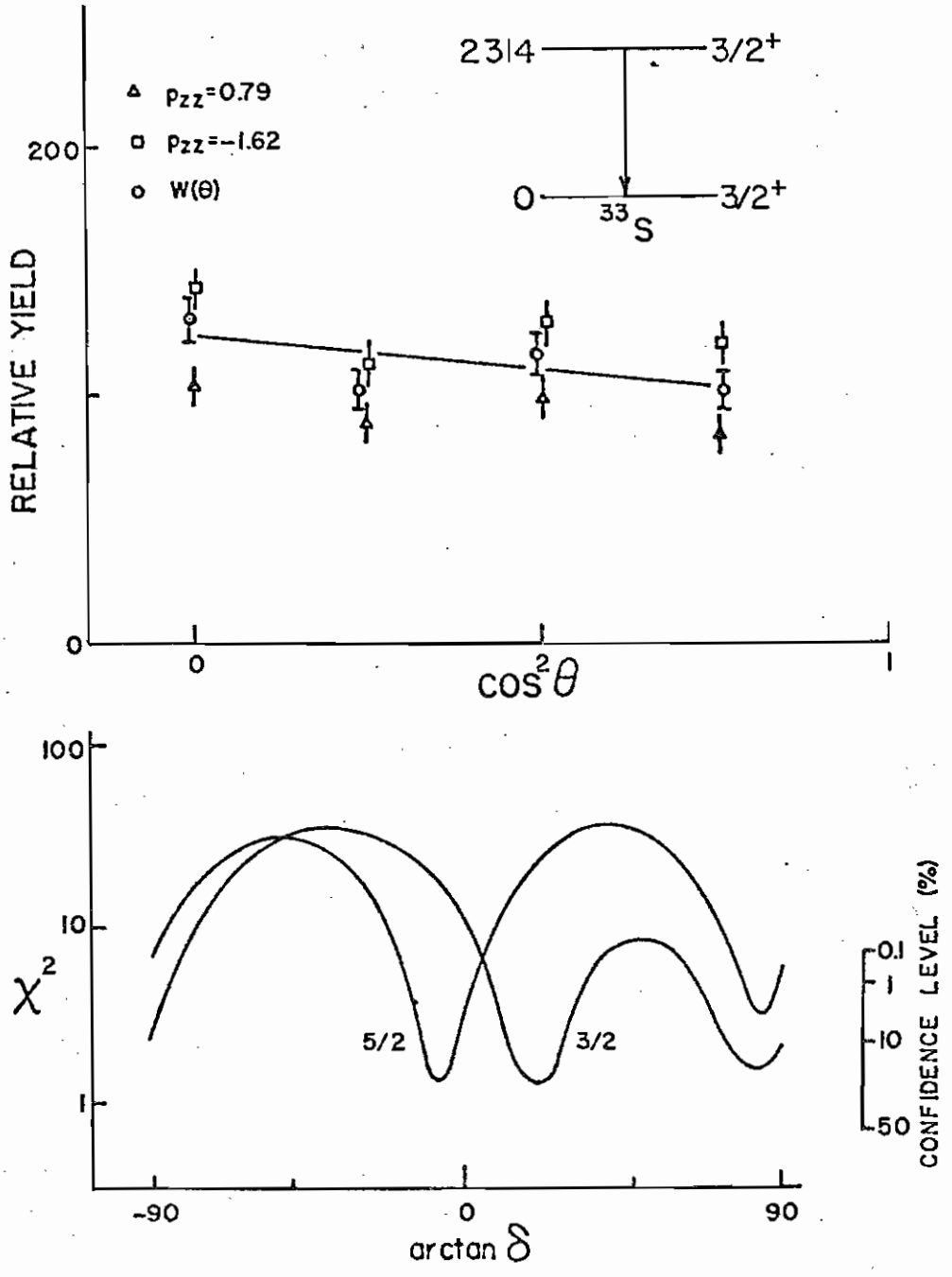
2314
3/2+
0
3/2+
33S
Pzz=0.79
Pzz=-1.62
W(θ)
200
0
RELATIVE YIELD
0
1
cos²θ
100
10
1
χ²
5/2
3/2
-90
0
90
arctan δ
0.1
1
10
50
CONFIDENCE LEVEL (%)

4) The 2868 keV Level

The angular correlations and X^2 fits to the data for this level are shown in Figure 11. The lower part of the figure shows plots of X^2 versus arctan δ for spin hypotheses 3/2 and 5/2. Spin hypotheses 7/2 and 9/2 have X^2 minima of 42 and 54 and are not shown. A spin assumption of J=1/2 yields minimum X^2=5. The 2868 keV level has been found to have $\ell_n = 2$ character in both stripping (17) and pickup (16) reactions. This limits the possible J^π to $3/2^+$ and $5/2^+$. This agrees with the present results where excellent fits to the data exist for both 3/2 and 5/2 spin assumptions. The values of δ corresponding of the X^2 minima are shown in Table 1: δ=0.43±0.07 or $6.5^{+4.6}_{-1.9}$ for J = 3/2, and δ = 0.088±0.040 for J = 5/2. These results are in excellent accord with values of δ = 0.47 or 5.7 (J=3/2) and δ=0.09 (J=5/2) measured by Carr, et. al.(5). Carr, et. al. (5) measured γ-ray angular distributions in singles using the $^{30}Si(\alpha, n\gamma)^{33}S$ reaction and a Ge(Li)-NaI(Tl) escape-suppressed and pair escape spectrometer. Their work used essentially the same technique employed by Ref. (23)---they have extended the work to higher lying levels. Carr, et. al. present an argument based on a comparison with ^{33}Cl which proposes that the 2868 keV level in ^{33}S is the mirror level of the 2848 keV state in ^{33}Cl, and thus probably $5/2^+$. Their data, however, presents the same conclusion as the present study---both J=3/2 and J=5/2 are equally likely spin hypotheses. As shown in Table 1, there is no reason based on transition strength systematics to favor 3/2 or 5/2.

Figure 11. Angular correlation results for the ground state transition from the 2868 keV level in ^{33}S. The lower part of the figure shows plots of X^2 versus arctan δ for J=3,5/2. The upper part of the figure shows the angular correlation data. Square and triangular points represent the two experimental correlations taken with differing p_{zz}. Circular points represent the combined correlation that is fitted to the theoretical expression. The line shown is the best least-squares fit, and is identical for J=3/2 or J=5/2.

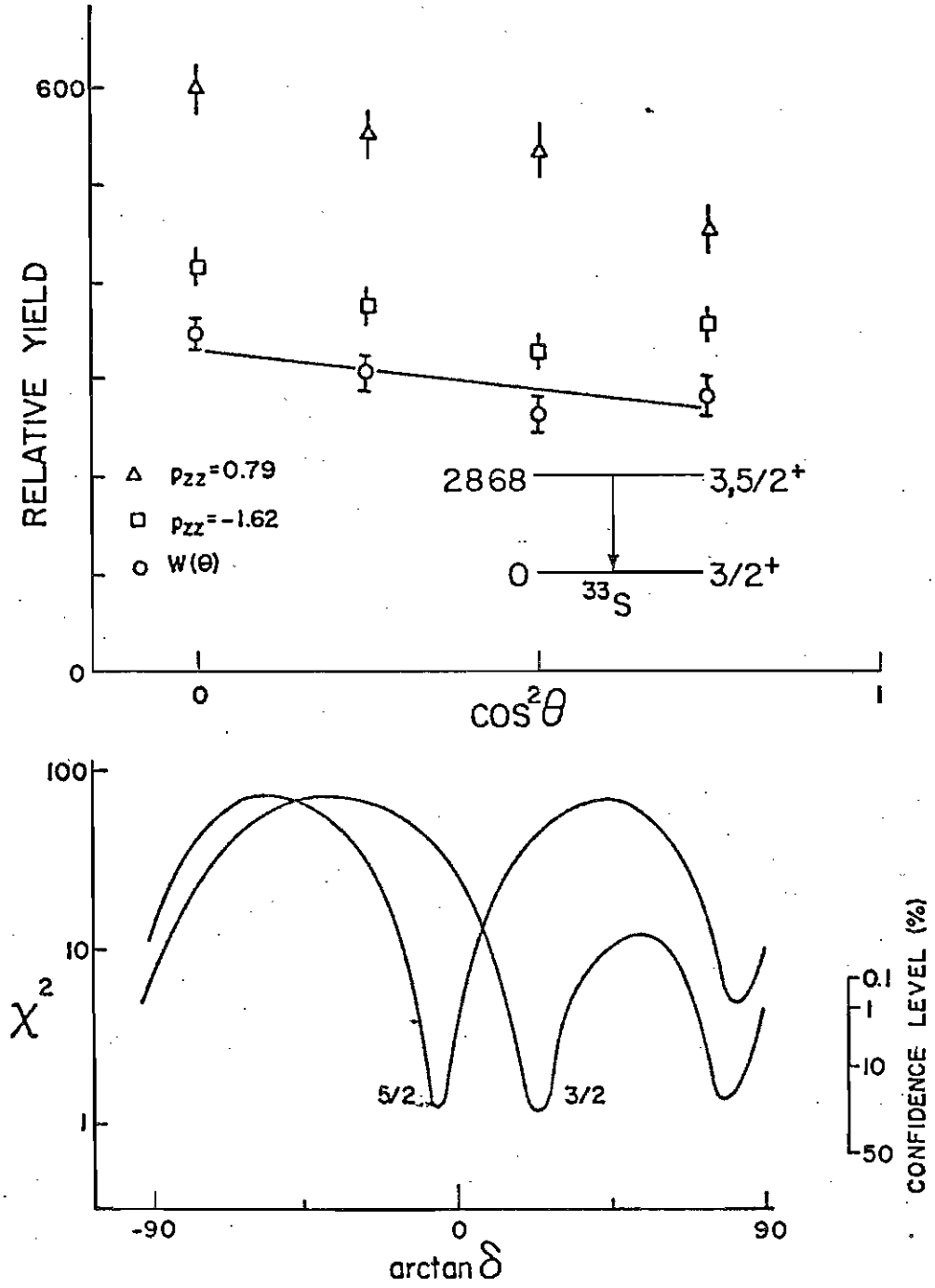
600
RELATIVE YIELD
0
0
1
cos²θ
Δ pzz=0.79
□ pzz=-1.62
○ W(θ)
2868
3,5/2⁺
0
3/2⁺
33S
100
10
1
χ²
5/2
3/2
-90
0
90
arctan δ
0.1
1
10
50
CONFIDENCE LEVEL (%)

5) The 2935, 2971, and 3221 keV Levels

These levels were not analyzed in this experiment. The 2935 and 2971 keV levels were unresolved in the proton spectrum, as shown in Figure 6. Since both have significant ground state decay branches an analysis of either level was not feasible. The 3221 keV level was not sufficiently populated for accurate analysis.

6) The 3833 keV Level

The angular correlations and X^2 fits for this level are shown in Figure 12. Spin hypotheses of J=1/2 through 9/2 all gave fits which approached the 0.1% confidence limit at some point. The lower part of Figure 12 shows fits for J=3/2 and J=5/2 due to the known ℓ_n=2 character of this level (16). As shown in Table 1, δ = 0.097±0.113 or $-3.5^{+1.3}_{-4.2}$ for a J=3/2 spin assumption, and δ=-0.36±0.12 for a J=5/2 spin assumption. These results are in excellent agreement with the results of $0.13 > \delta > -8.14$ for J=3/2 and δ=-0.41±0.17 for J=5/2 measured by Carr, et. al. (5). The present results for J=3/2 represents an improvement over previous work where the mixing ratio was only restricted in a very general way. The deep minimum in the X^2 fit for J=5/2 at arctan $\delta \approx -80°$ was not seen in the $(\alpha, n\gamma)$ work (5) and is not listed as a possible solution in Table 1 for this reason. Referring to the E2 and M1 transition strengths in Table 1, it is apparent that the present work cannot resolve the 3/2,5/2 ambiguity in the spin assignment.

Figure 12. Angular correlation results for the ground state transition from the 3833 keV level in ^{33}S. The lower part of the figure shows plots of X^2 versus arctan δ for J=3,5/2. The upper part of the figure shows the angular correlation data. Square and triangular points represent the two experimental correlations taken with differing p_{zz}. Circular points represent the combined correlation that is fitted to the theoretical expression. The lines shown are best least-squares fits for J=3/2 and J=5/2, as shown.

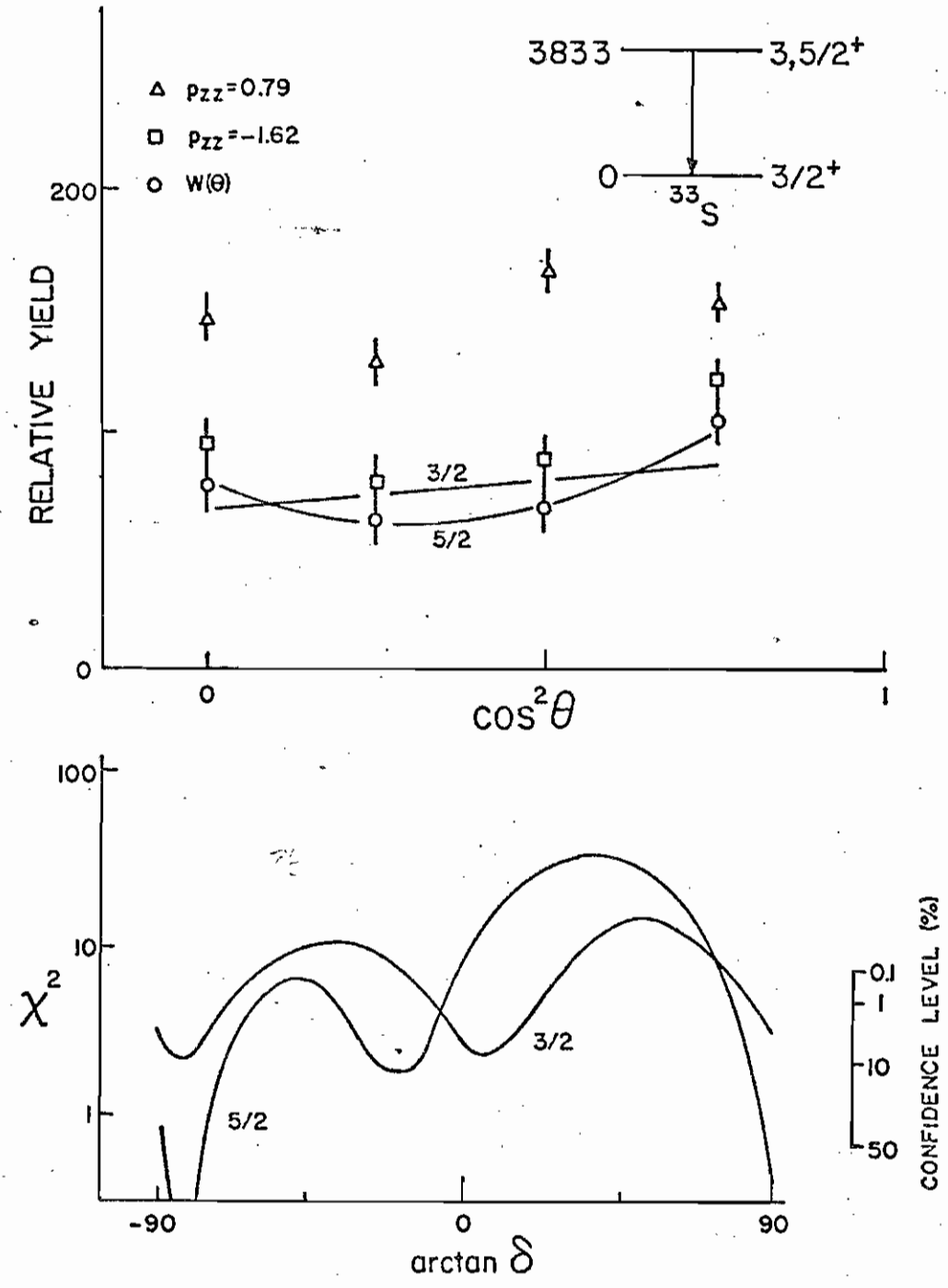
3833
3,5/2+
0
3/2+
33S
Δ pzz=0.79
□ pzz=-1.62
○ W(θ)
200
RELATIVE YIELD
3/2
5/2
0
1
cos²θ
100
10
1
χ²
3/2
5/2
-90
0
90
arctan δ
0.1
1
10
50
CONFIDENCE LEVEL (%)

Table 1. Summary of experimental results for ^{33}S with comparisons to previous measurements by (5) and (23). E_x, previous δ, τ_m and B.R. are from (5,23). Transition matrix elements are calculated based on the current measurement of δ.

^{33}S EXPERIMENTAL RESULTS

E_x (keV)	J^π	B.R. (%)	τ_m (fs)	Previous δ	This δ	$\lvert M\rvert^2$ M1	$\lvert M\rvert^2$ E2
1968.0±0.6	$5/2^+$	100	189±16	0.56±0.18	0.34±0.13	$(2.0\pm0.4)\times10^{-2}$	2.4±2.0
2313.7±0.5	$3/2^+$	30±4	198±9	0.28±0.08	0.38±0.10	$(3.4\pm0.8)\times10^{-3}$	0.37±0.23
				>11.4	9^{+38}_{-4}	$(0.47^{+0.50}_{-4.0})\times10^{-4}$	$2.9^{+0.8}_{-0.6}$
2868.2±0.3	$3/2^+$	100	34±11	0.47±0.13	0.43±0.07	0.033±0.014	3.1±2.0
				$5.7^{+8.6}_{-3.5}$	$6.5^{+4.6}_{-1.9}$	$(0.91^{+0.86}_{-1.6})\times10^{-3}$	19.2±7.5
	$5/2^+$			-0.09±0.04	-0.088±0.040	0.039±0.013	0.15±0.18
3833.0±1.0	$3/2^+$	100	44±4	$0.13>\delta>-8.1$	0.097±0.113	$(1.3\pm0.2)\times10^{-2}$	$(3.3\pm8.1)\times10^{-2}$
					$-3.5^{+1.3}_{-4.2}$	$(0.97\pm2.2)\times10^{-3}$	$3.3^{+0.90}_{-1.0}$
	$5/2^+$			-0.41±0.17	-0.36±0.12	$(1.1\pm0.2)\times10^{-2}$	0.41±0.30

B. Results for ^{35}S

It is more difficult to obtain electronic transition strengths for the γ-ray decays of the levels in ^{35}S than for ^{33}S. No correlation experiments have been performed which rigorously restrict the population of the magnetic substates, although some work has been done via the $^{34}S(d,p\gamma)^{35}S$ reaction with unpolarized deuteron beams. Two recent experiments have been carried out via this reaction at Groningen and at Strasbourg. The first and earlier of these was performed by van der Mark and ter Veld (30) using both the $^{34}S(d,p\gamma)^{35}S$ and the $^{37}Cl(d,\alpha\gamma)^{35}S$ reactions. Their experiment with the (d,pγ) reaction employed Litherland and Ferguson's co-linear geometry (41) by detecting γ-rays in a 7.6 x 7.6 cm NaI detector in coincidence with protons detected in an annular surface barrier detector. With a deuteron beam energy of E_d=4.72 MeV and a target thickness of ≃80 μg/cm^2, their experiment was similar to the present work with the important exception of the polarized beam. (The deuteron beam energy for the present work was chosen after a singles particle excitation function experiment revealed that E_d = 4.7 MeV was the best energy for population of the upper levels of interest.) Van der Mark and ter Veld also performed a (d,αγ) experiment using a 120 cm^3 Ge(Li) detector with the co-linear geometry. With this arrangement a new level was found and since confirmed(28) at E_x=3821 keV.

The later of the two measurements on ^{35}S discussed here was made by Freeman, Faerber, Toulemonde, and Gallman at Strasbourg (28).

Figure 13. Coincident proton spectrum for the $^{34}S(\vec{d},p\gamma)^{35}S$ reaction at $E_d = 4.72$ MeV. Numbers labeling the peaks are the excitation energies of the levels in ^{35}S in keV.

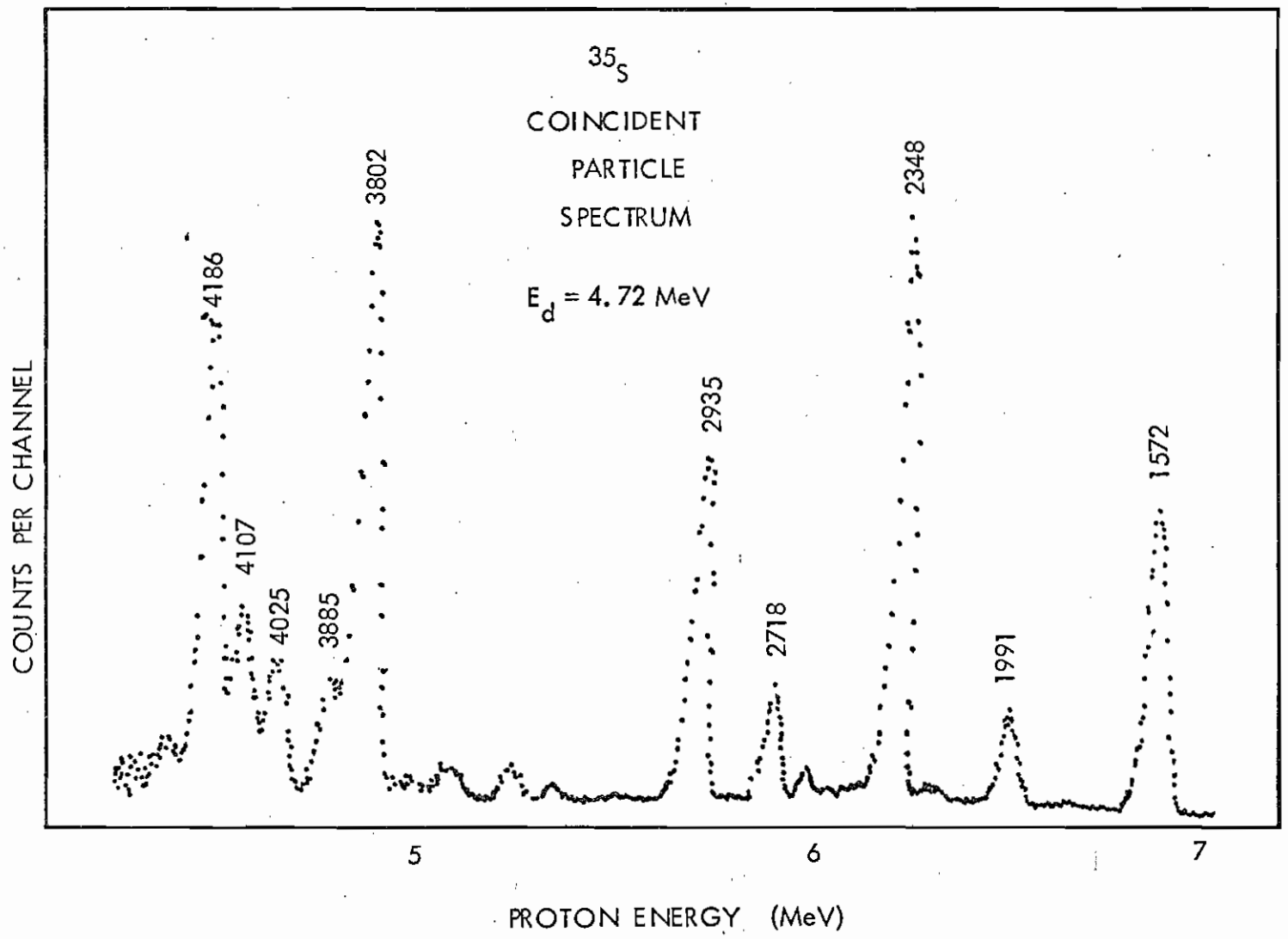
^{35}S
COINCIDENT
PARTICLE
SPECTRUM
E_d = 4.72 MeV
4186
4107
4025
3885
3802
2935
2718
2348
1991
1572
COUNTS PER CHANNEL
5
6
7
PROTON ENERGY (MeV)

Figure 14. Energy level diagram for ^{35}S. E_x and τ_m are taken from (28).

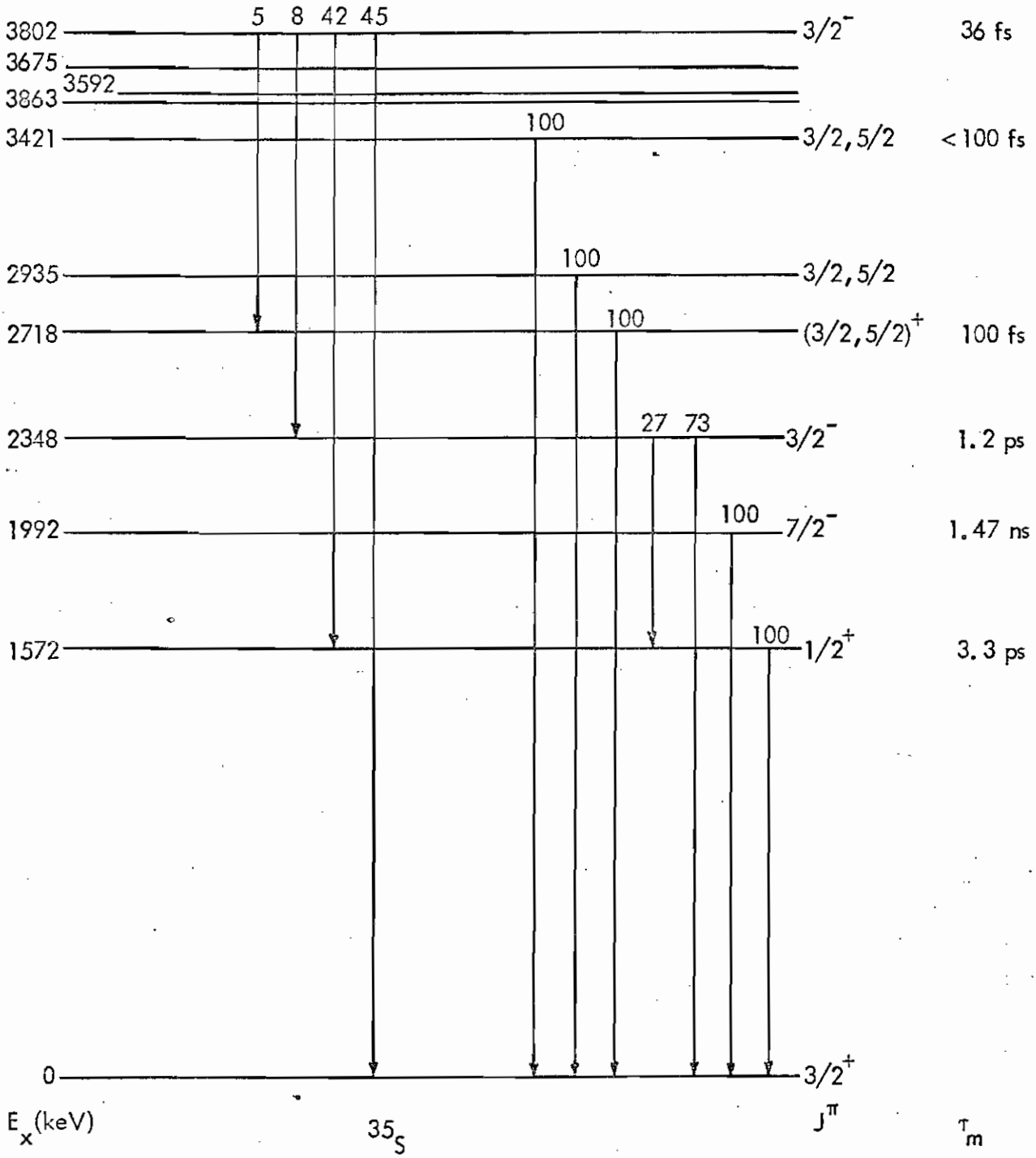
3802
3675
3592
3863
3421
2935
2718
2348
1992
1572
0
5 8 42 45
100
100
100
27 73
100
100
3/2⁻
3/2,5/2
3/2,5/2
(3/2,5/2)⁺
3/2⁻
7/2⁻
1/2⁺
3/2⁺
36 fs
< 100 fs
100 fs
1.2 ps
1.47 ns
3.3 ps
E_x(keV)
35S
J^π
τ_m

Freeman, et. al. made lifetime and angular correlation measurements via the $^{34}S(d,p\gamma)^{35}S$ reaction using the co-linear geometry technique (41). Targets of 550 $\mu g.cm^2$ $Sb^{34}S$ were bombarded with incident deuteron beams of 3.5 and 4.0 MeV energy. Gamma rays were detected in a 40 cm^3 Ge(Li) detector in coincidence with protons detected in an annular detector placed at 180° to the beam. Their experimental technique and apparatus are very similar to that of van der Mark and ter Veld and to the present work. The central difference between previous work and the present work is, of course, the polarized beam.

1) The 1572 keV Level

The angular correlations and X^2 analysis for this level are shown in Figure 15. The lower part of the figure displays plots of X^2 versus arctan δ for spin hypotheses of 1/2, 3/2, and 5/2. Analyses for J=7/2 and 9/2 did not exceed the 0.1% confidence limit and are not shown. As seen in the upper half of the figure the angular correlation is isotropic within statistical errors. This result is in agreement with the known (24) $J^{\pi} = 1/2^+$ nature of this level. As shown in Section II.C., no mixing ratio information is obtainable for a J=1/2 level using the co-linear angular correlation technique (41).

2) The 1991 keV Level

The angular correlations and X^2 analyses for this level are shown in Figure 16. Results of the theoretical fits to the data are shown for spin

Figure 15. Angular correlation results for the 1572 keV level in ^{35}S. The lower part of the figure shows plots of X^2 versus arctan δ for J=1,3,5/2. The upper part of the figure shows the angular correlation data. Square and triangular points represent the two experimental correlations taken with differing p_{zz}. Circular points represent the combined correlation that is fitted to the theoretical expression. The line shown is the best least-squares fit to the data for J=1/2.

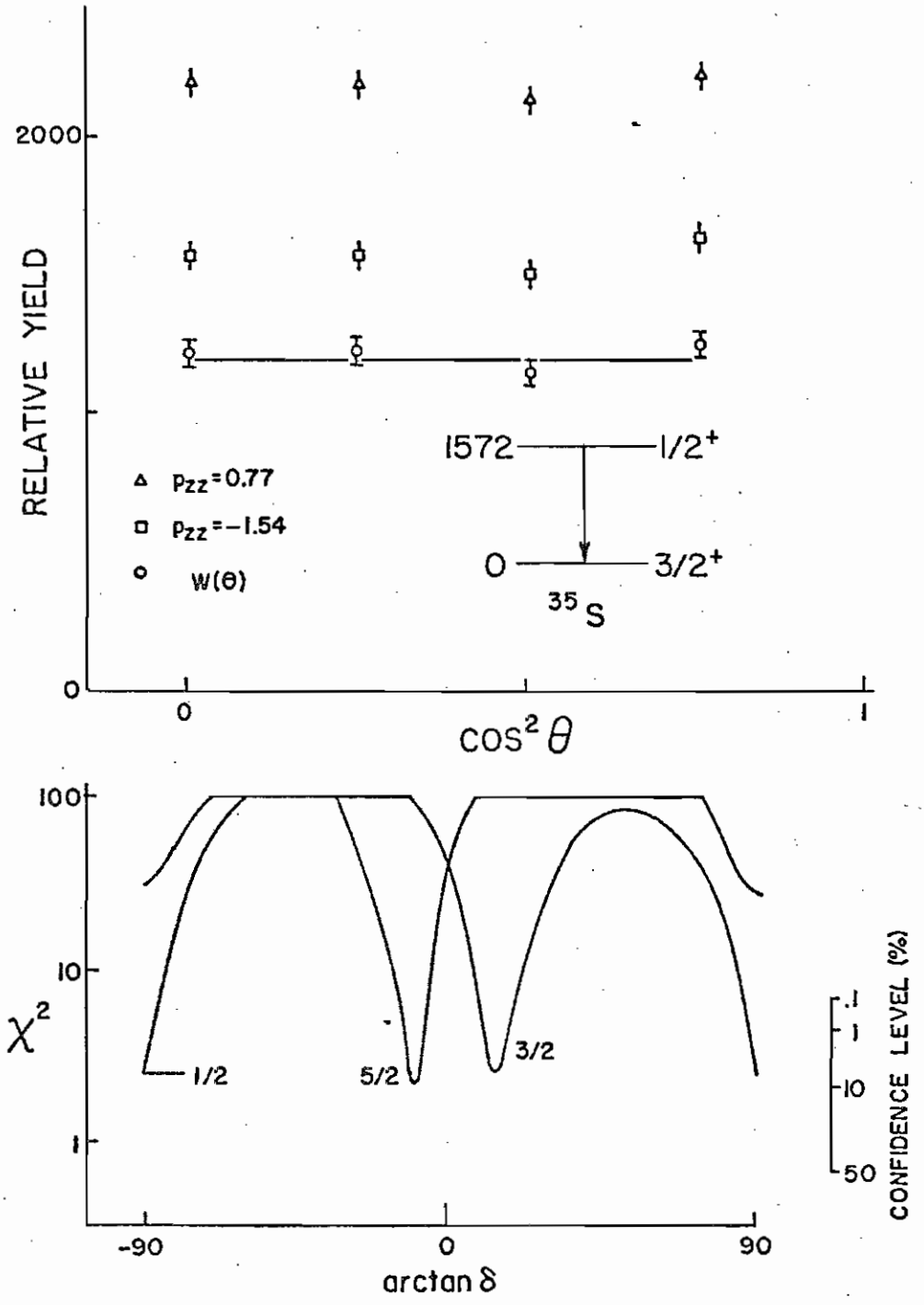
RELATIVE YIELD
2000
0
0
1
cos² θ
Pzz=0.77
Pzz=−1.54
W(θ)
1572
1/2⁺
0
3/2⁺
35S
100
10
1
χ²
1/2
5/2
3/2
-90
0
90
arctan δ
CONFIDENCE LEVEL (%)
.1
1
10
50

Figure 16. Angular correlation results for the ground state transition from the 1991 keV level in ^{35}S. The lower part of the figure shows plots of X^2 versus arctan δ for J=5,7/2. The upper part of the figure shows the angular correlation data. Square and triangular points represent the two experimental correlations taken with differing p_{zz}. Circular points represent the combined correlation that is fitted to the theoretical expression. The line shown is the best least-squares fit to the data for J=7/2.

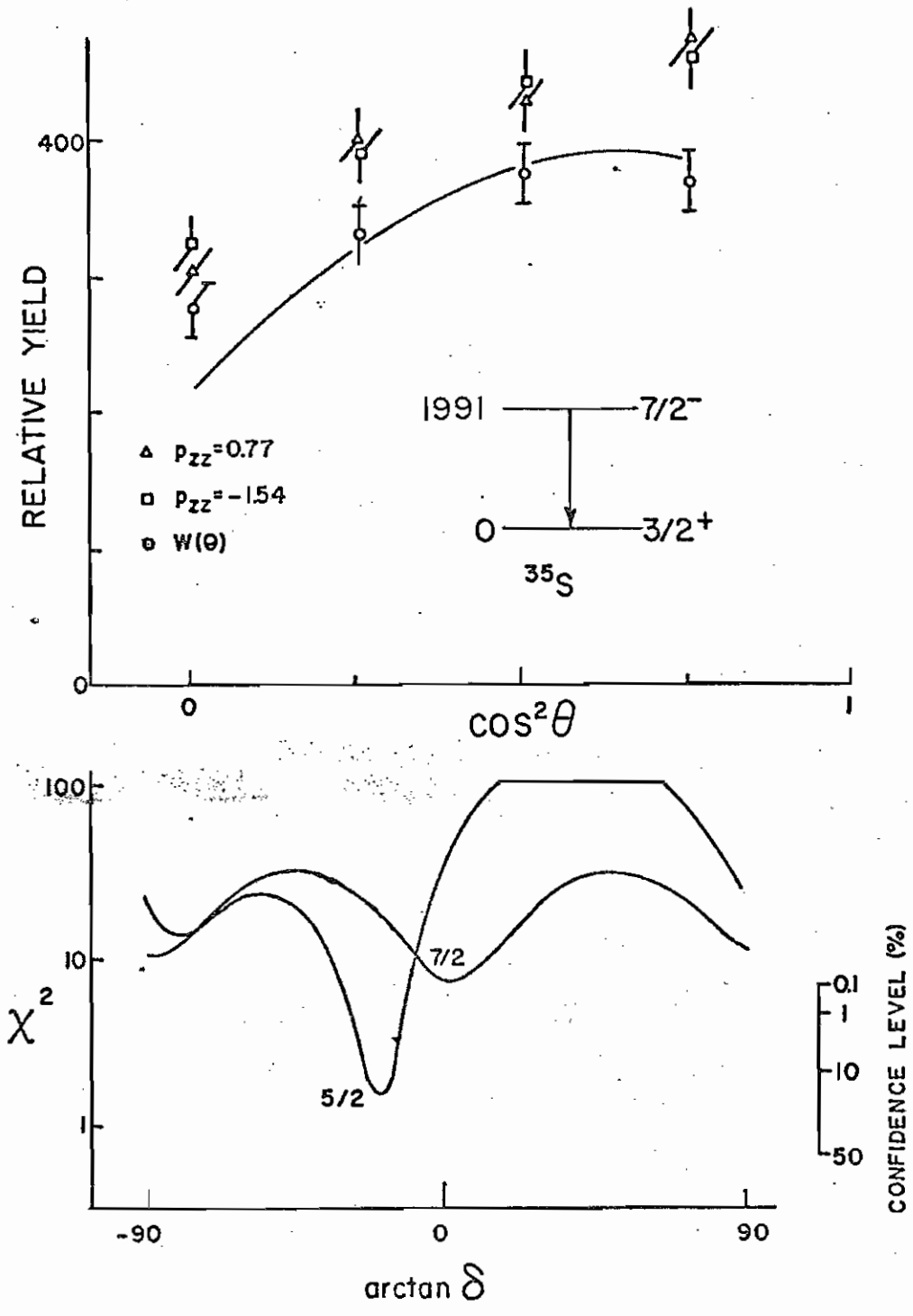
RELATIVE YIELD
400
0
0
1
cos²θ
△ p_{zz}=0.77
□ p_{zz}=-1.54
● W(θ)
1991
7/2⁻
0
3/2⁺
35S
100
10
1
χ²
7/2
5/2
-90
0
90
arctan δ
CONFIDENCE LEVEL (%)
0.1
1
10
50

hypotheses of J=5/2 and J=7/2 consistent with the known ℓ_n=3 character of this level (26). Other X^2 fits are omitted for clarity. As shown in the lower half of the figure the J=5/2 spin hypothesis has a much deeper X^2 minimum than the J=7/2 fit, which only just reaches the 0.1% confidence level. A spin of 5/2 would imply a mixing ratio of δ=-0.35±0.03, while a J=7/2 assumption would mean that δ = 0.042±0.050. If the spin of this level were $5/2^-$, the large measured value of the multipole mixing ratio would imply an E1 transition strength of 7×10^{-8} W.u., as shown in Table 2. This value would be abnormally small but not unknown (64). Almost all E1 strengths in this mass region fall in the range of 10^{-6} to 10^{-2} W.u. There is only one measured E1 transition strength tabulated by Endt and van der Leun (64) that is within a factor of 10 of the 1991 keV($5/2^-$) strength (^{22}Ne, 5.14--1.27 MeV, B(E1)=1.4×10^{-8}W.u.). This fact would tend to discourage an assignment of $J=5/2^-$. The alternative hypothesis of $J=7/2^-$ implies transition strengths of 0.23 and 0.09 W.u. for the E3 and M2 components, respectively.

The result of the present experiment of δ = -0.35 for J=5/2 is in fairly good agreement with the result of δ=-0.43 obtained by van der Mark and ter Veld (30). The present measurement of δ=0.042 for $J^\pi=7/2^-$ should be compared with the measurement of δ=0.28 by van der Mark and ter Veld(30) and the measurement of δ=0.11 by Freeman, et. al.(28). The present work agrees with the results of Freeman, et. al. but disagrees with the results of van der Mark and ter Veld. Some disagreement with the present data would perhaps not be surprising because (see Figure 16) the J=7/2 X^2 fit is very poor.

An explanation for this problem might be the unusually long lifetime (1.47 ns) of this level, which might allow the orientation of the recoiling nucleus to become perturbed, thus attenuating the angular correlation. This possibility has been discussed by both Freeman, et. al. and van der Mark and ter Veld, but a conclusion is difficult to come by. The spin of the 1991 keV level is most probably $7/2^-$, but the interpretation of the multipole mixing ratio measurements is somewhat difficult.

3) The 2348 keV Level

The angular correlations and X^2 analyses for this level are shown in Figure 17. The present analysis yields $\delta=0.044\pm0.021$ for a spin hypothesis of J=3/2. This result is in excellent agreement with a previous measurement of $\delta = 0.01\pm0.04$ by Freeman, et. al.(28) and in poor agreement with the value of $\delta =-0.27\pm0.12$ obtained by van der Mark and ter Veld. This level is known to be $J^\pi=3/2^-$, and both previous measurements were made by simultaneously fitting correlations for two de-excitation γ-rays. Freeman, et. al. analyzed the ground state transition by assuming the transition to the 1572 keV first excited state was of pure E1 character. Van der Mark and ter Veld fitted multipole mixing ratios for both transitions simultaneously. This situation represents an excellent example of the applicability of the $(\vec{d},p\gamma)$ polarized beam angular correlation method. The analysis in the present case was made by fitting the 75% ground state branch alone. The value of $\delta=0.044$ yields M2/E1 transition strengths of $0.067/\ 4.2\times10^{-5}$ W.u., as shown in Table 2.

Figure 17. Angular correlation results for the ground state transition from the2348 keV level in ^{35}S. The lower part of the figure shows plots of X^2 versus arctan δ for J=3, 5/2. The upper part of the figure shows the angular correlation data. Square and triangular points represent the two angular correlations taken with differing p_{zz}. Circular points represent the combined correlation that is fitted to the theoretical expression. The line shown is the best least-squares fit to the data for J=3/2.

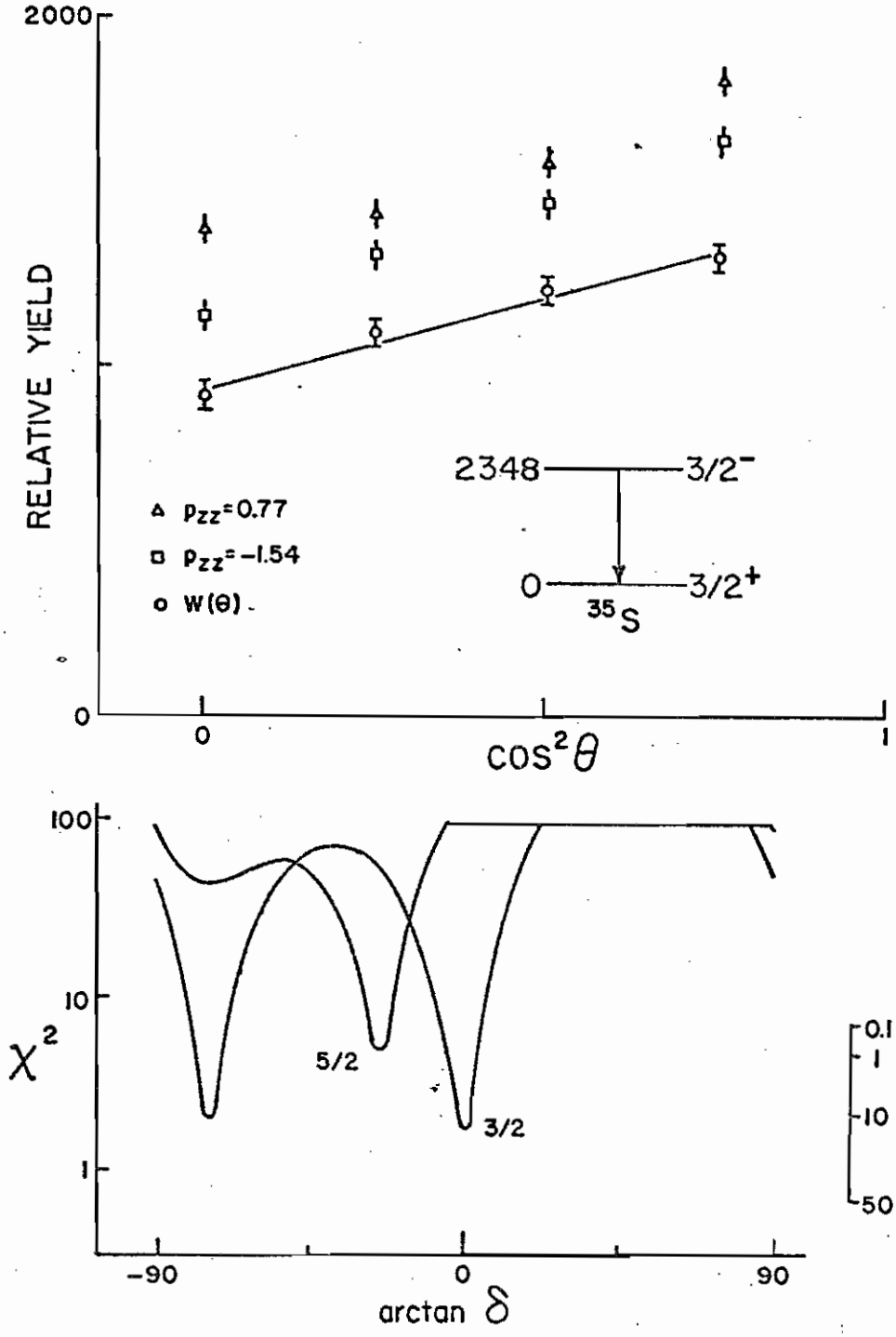
2000
RELATIVE YIELD
0
0
1
cos²θ
△ pzz=0.77
□ pzz=-1.54
○ W(θ)
2348
3/2⁻
0
3/2⁺
35S
100
10
1
χ²
5/2
3/2
-90
0
90
arctan δ
0.1
10
50
CONFIDENCE LEVEL (%)

4) The 2718 keV Level

Angular correlations and X^2 analyses for this level are shown in Figure 18. Plots of X^2 versus arctan δ are shown in the lower part of the figure for J=3/2 and J=5/2 as this level is known to have ℓ_n=2. Results for other spin assumptions are omitted for clarity. The data for this level allows two solutions for the mixing ratio for both J=3/2 and J=5/2. For a J=3/2 spin assumption, δ=0.065 implies E2/M1 transition strengths of 0.034/0.016 W.u., while δ=-5.4 would imply E2/M1 strengths of $7.8/5.2\times10^{-3}$ W.u. For an assumed J = 5/2, δ=-0.36 implies E2/M1 strengths of 0.94/0.014 W.u., while the alternative δ=-7.1 implies E2/M1 transition strengths of $7.9/3\times10^{-4}$ W.u. The systematics of this mass region as compiled by Endt and van der Leun (64) show that M1 strengths fall in the general range of 10^{-4} to 10 W.u. while E2 strengths fall in the range of 10^{-2} to 10^{2} W.u. It is apparent from this that all four of the possible mixing ratios measured give reasonable results for the transition strengths. None of the possible solutions for δ can be excluded. An example of the advantages of the polarized beam can be seen by comparing the X^2 versus arctan δ plot for J=3/2 in Figure 18 with the equivalent diagram in van der Mark and ter Veld's work (Figure 3b, page 201, Ref. (30)). Without the use of the polarized beam, virtually no mixing ratio information can be extracted.

5) The 2935 keV Level

Angular correlations and X^2 analyses are shown for this level in Figure

Figure 18. Angular correlation results for the ground state transition from the 2718 keV level in ^{35}S. The lower part of the figure shows plots of X^2 versus arctan δ for J=3, 5/2. The upper part of the figure shows the angular correlation data. Square and triangular points represent the two experimental correlations taken with differing p_{zz}. Circular points represent the combined correlation that is fitted to the theoretical expression. The line shown is the best least-squares fit to the data for J=5/2.

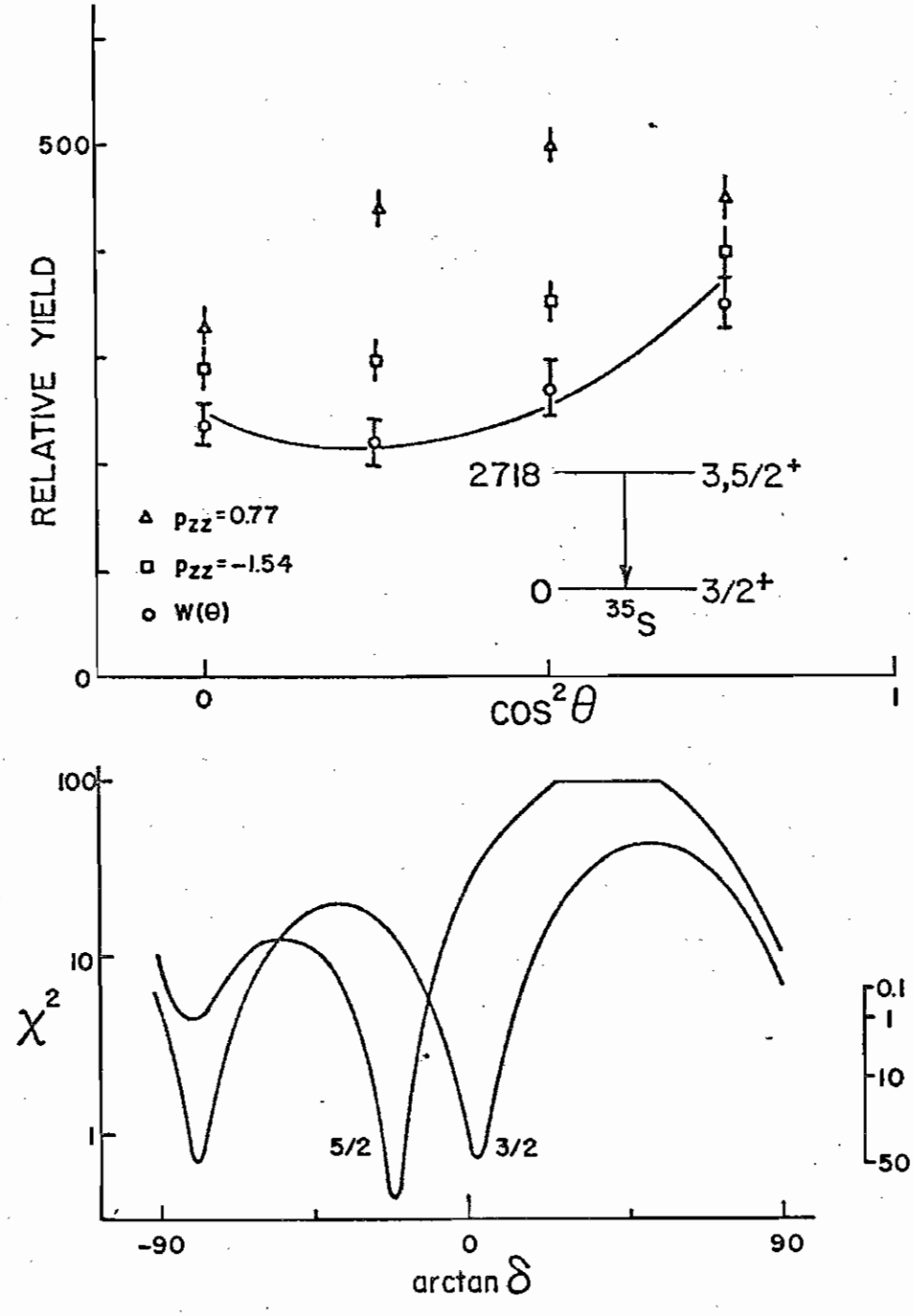
RELATIVE YIELD
500
0
0
1
cos²θ
△ Pzz=0.77
□ Pzz=-1.54
○ W(θ)
2718
3,5/2⁺
0
3/2⁺
35S
χ²
100
10
1
5/2
3/2
-90
0
90
arctan δ
CONFIDENCE LEVEL (%)
0.1
1
10
50

Figure 19. Angular correlation results for the ground state transition from the 2935 keV level in ^{35}S. The lower part of the figure shows plots of X^2 versus arctan δ for J=3,5/2. The upper part of the figure shows the angular correlation data. Square and triangular points represent the two experimental correlations taken with differing p_{zz}. Circular points represent the combined correlation that is fitted to the theoretical expression. The line shown is the best least-squares fit for both J=5/2 and J=3/2.

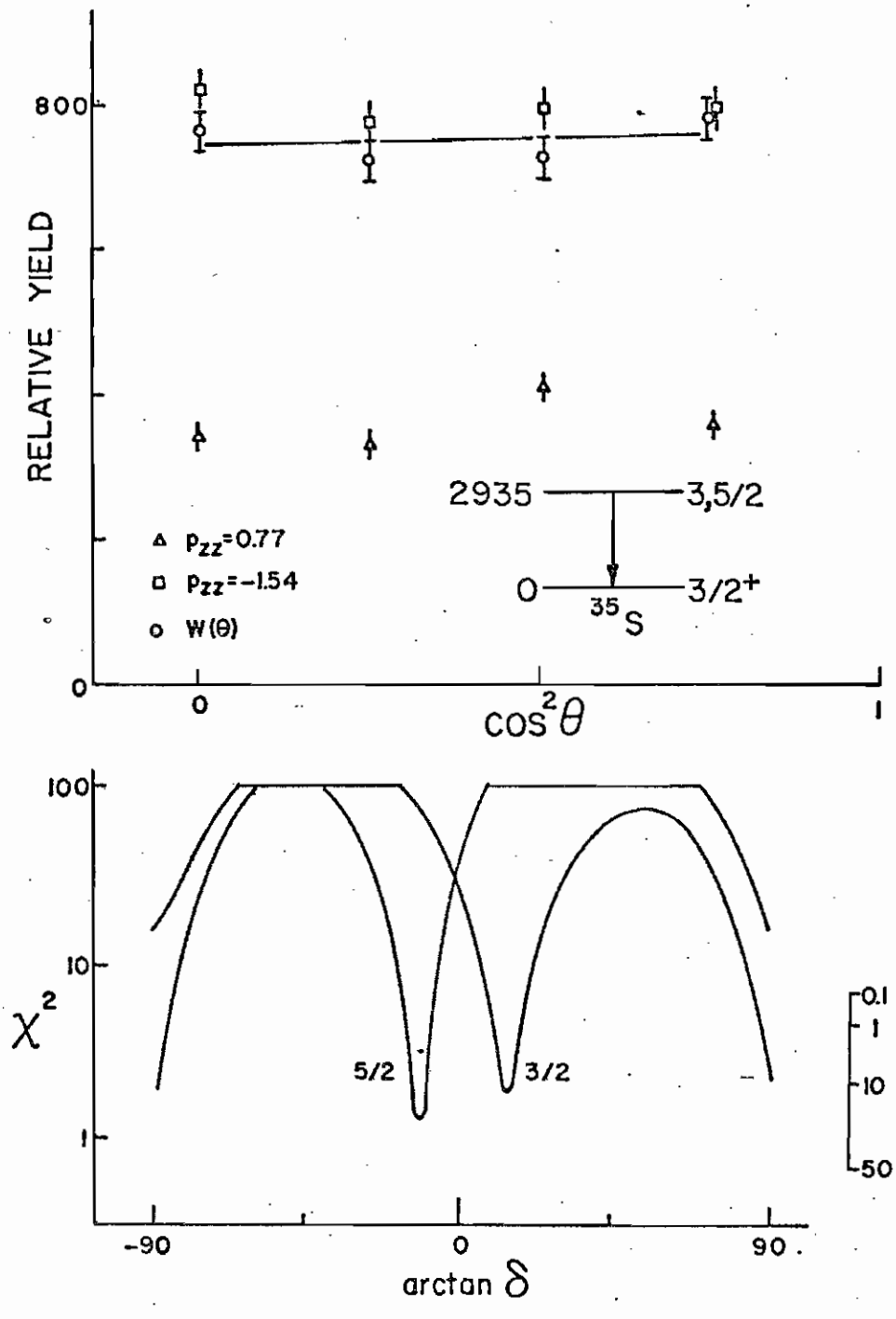
800
RELATIVE YIELD
0
0
cos²θ
1
△ p_{zz}=0.77
□ p_{zz}=-1.54
○ W(θ)
2935
3,5/2
0
3/2⁺
35S
100
10
1
χ²
5/2
3/2
-90
0
90
arctan δ
0.1
1
10
50
CONFIDENCE LEVEL (%)

19. The results of the present investigation confirm previous work (28) assigning this level J=3/2,5/2. As shown in Table 2, a spin 3/2 assumption implies δ=0.34 while a spin 5/2 assumption implies δ = -0.086. The mean lifetime of this level has never been measured, and thus no transition strenghts can be calculated.

6) The 3421, 3563, 3592, and 3675 keV Levels

These four levels are weakly excited with the (d,p) reaction. In addition, the proton group corresponding to the 3421 keV level lies very close to the $^{12}C(d,p)^{13}C$ ground state group. This carbon group became stronger as the measurements progressed, reflecting carbon buildup on the target. This made analysis of the 3421 keV level uncertain. The 3563 and 3593 keV proton groups were unresolved in the particle spectrum and since the decay scheme of the 3563 keV level is not well understood (28) an analysis was not attempted. The 3675 keV level was not populated sufficiently for significant data to be accumulated.

7) The 3802 keV Level

Angular correlations and X^2 fits for this level are shown in Figure 20. The level is known to be $J^{\pi} = 3/2^-$ and the present data for this spin assumption allow two possible values of the mixing ratio, one of which can be ruled out by systematics considerations. As shown in Table 2 the larger value of δ = -8 implies an M2 transition strength of 65 W.u. Taking the possible error into account, the lowest probable strength for the M2 transition

Figure 20. Angular correlation results for the ground state transition from the 3802 keV level in ^{35}S. The lower part of the figure shows plots of X^2 versus arctan δ for J=3,5/2. The upper part of the figure shows the angular correlation data. Square and triangular points represent the two experimental correlations taken with differing p_{zz}. Circular points represent the combined correlation that is fitted to the theoretical expression. The line shown is the best least-squares fit to the data for J=3/2.

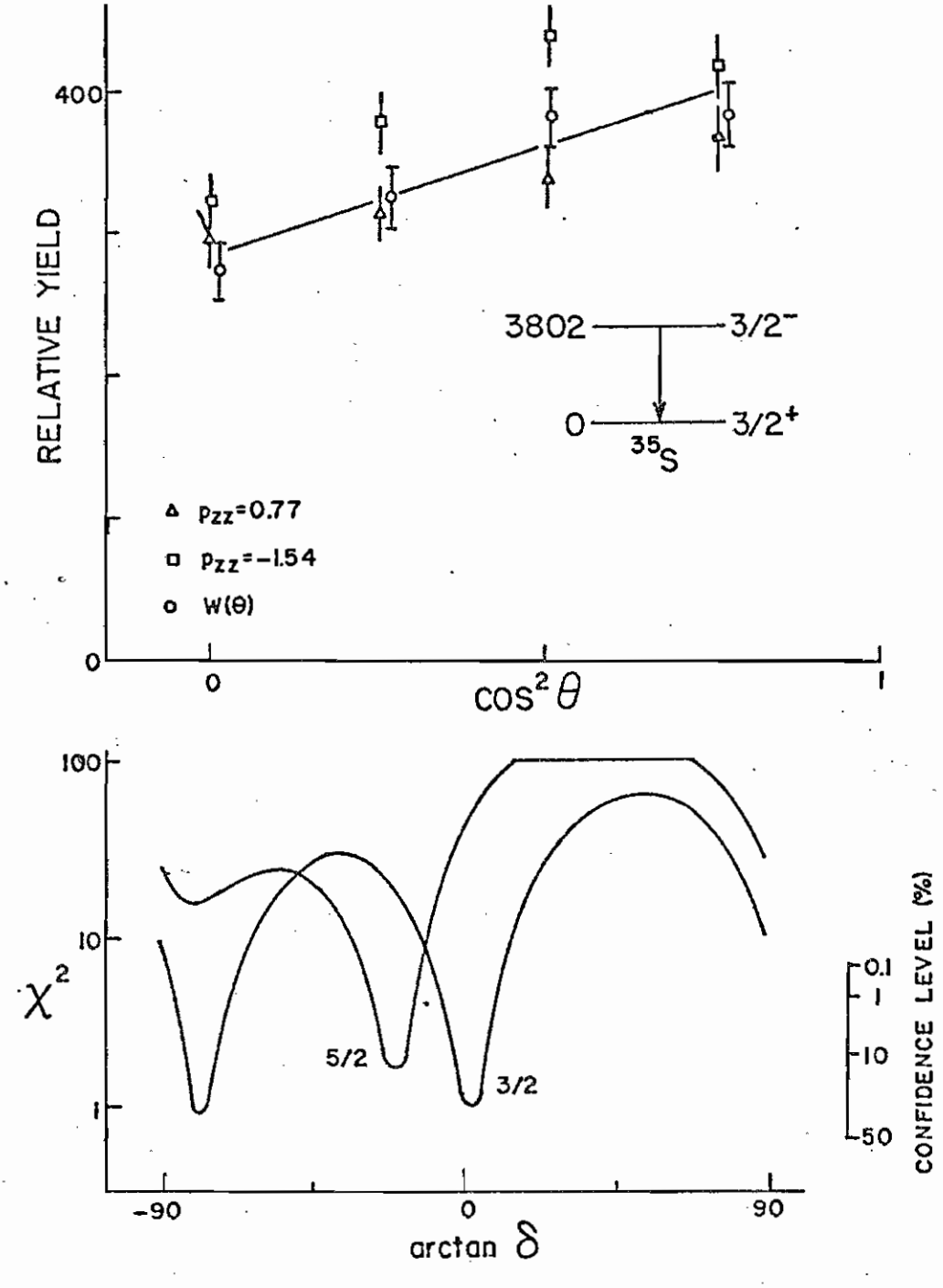
400
RELATIVE YIELD
0
0
cos² θ
1
3802
3/2⁻
0
3/2⁺
35S
△ Pzz=0.77
□ Pzz=-1.54
○ W(θ)
100
10
1
χ²
5/2
3/2
-90
0
90
arctan δ
0.1
1
10
50
CONFIDENCE LEVEL (%)

matrix element is 12 W.u. Endt and van der Leun (64) suggest that the upper limit for a M2 transition strength be 3 W.u.. This is a factor of 4 smaller than the smallest value of the measurement, and the value of $\delta = -8$ is thus excluded. The probable value of the mixing ratio is thus taken to be $\delta = 0.18$ with corresponding M2/E1 transition strengths of $2/2 \times 10^{-4}$ W.u. Note that this level was analyzed unambiguously even though the 3802 and 3815 keV levels were not resolved in the proton spectrum because, 1) the 3802 keV level has a relatively high yield, and 2) the 3815 keV level decays 100% to the first excited state (28). The 3802 keV ground state decay was thus analyzed free of interference.

Table 2. Summary of experimental results for ^{35}S. E_x, τ_m and B.R.'s are taken from (28). Mixing ratios and transition rates shown are the results of the present experiment.

^{35}S EXPERIMENTAL RESULTS

E_x (keV)	J^π	B.R. (%)	T_m	δ 4 detectors	δ 5 detectors	δ average	Multipolarity	B(L) / B(L+1)
1991.2±0.3	$(5/2^-)$	100	1.47 ± 0.07 ns	-0.33 ± 0.04 -0.37 ±0.05		-0.35 ±0.03	E1 M2	$(7.0\pm0.6)\times10^{-8}/0.01\pm0.002$
	$7/2^-$			0.059±0.067 0.022±0.075		0.042±0.050	M2 E3	(0.09±0.006)/0.23±0.56
2347.5±0.2	$3/2^-$	73 ± 2	1.22 ± 0.18 ps	0.11 ±0.03 -0.018±0.028	0.042±0.049	0.044±0.021	E1 M2	$(4.2\pm0.7)\times10^{-5}/(6.7\pm7.6)\times10^{-2}$
2718.0±1.0	$3/2^+$	100	100 ± 35 fs	0.19 ±0.07 0.003±0.062	-0.053±0.134	0.065±0.054	M1 E2	0.016±0.006/0.034±0.068
	$3/2^+$			$-16.3^{+8.5}_{-259.}$ $-3.9^{+0.8}_{-1.4}$	$-3.2^{+1.0}_{-2.6}$	$-5.4^{+1.2}_{-2.4}$	M1 E2	$(5.2\pm0.6)\times10^{-3}/7.8\pm3.0$
	$5/2^+$			-0.24 ±0.06 -0.45 ±0.08	-0.58 ±0.22	-0.36 ±0.08	M1 E2	0.014±0.006/0.94±0.70
	$5/2^+$			-21^{+11}_{-141} $-4.3^{+0.9}_{-1.6}$	$-4.0^{+1.3}_{-3.7}$	$-7.1^{+1.9}_{-3.6}$	M1 E2	$(3.1\pm4.1)\times10^{-4}/7.9\pm3.0$
2935 ± 3	3/2	100		0.48 ±0.04 0.24 ±0.04	0.31±0.04	0.34 ±0.02		
	5/2			-0.06±0.02 0.21 ±0.03	0.16±0.03	0.086±0.015		
3802.0±1.0	$3/2^-$	45 ± 4	36 ± 26 fs	0.36 ±0.06 0.039±0.052	0.15 ±0.08	0.18 ±0.04	E1 M2	$(2.0\pm1.7)\times10^{-4}/2.0\pm2.4$
					$-9.2^{+3.9}_{-25.1}$	-8^{+2}_{-3}	E1 M2	$(3.2\pm5.1)\times10^{-5}/65\pm53$
				$-4.6^{+0.9}_{-1.5}$				

Chapter IV

DISCUSSION

A. Theory

The nuclei ^{33}S and ^{35}S are in an interesting region of the s-d shell, where much theoretical work has been done (see Ref. (5) and therein). Recently several calculations have been made for ^{33}S electromagnetic properties which compare well with available data. Castel, et. al. (49) performed detailed intermediate coupling calculations for ^{33}S and ^{34}S, some of the results of which are shown in Table 3. Groups at Utrecht (Glaudemans, et. al. (51)) and Oak Ridge (Wildenthal, et. al. (52)) have performed extensive and detailed shell model calculations with the modified surface delta interaction (MSDI) approach. Both calculations allow active $2s_{1/2}$, $1d_{3/2}$, and $1d_{5/2}$ (up to 2-hole excitations) orbitals. The Utrecht calculation involved 7 parameters (3 single-particle energies and 4 two-body interaction) determined by a least-squares fit to experimental excitation energies and ground state binding energies. These pre-fitted parameters were kept constant throughout the rest of the calculation. The Oak Ridge group performed a very similar calculation with the MSDI, and in addition performed a calculation referred to as FPSDI (free parameter surface delta interaction) which involved fitting 22 parameters instead of 7. The two-body matrix elements for the $2s_{1/2}$ and $1d_{3/2}$ orbits and the 3 single particle energies were refitted to experimental data resulting in better agreement with experiment in some instances (see (52),

page 1718).

Very few published calculations exist for ^{35}S and none exist that calculate detailed electromagnetic transition matrix elements. Wildenthal, et. al. (52) have studied A=35 nuclei but have calculated only spectroscopic factors, quadrupole moments, etc. for ^{35}S. The lack of experimental evidence is no doubt responsible for this. Calculations are planned in the future to remedy this lack of theoretical evidence.

The situation with ^{33}S is entirely different. Both recent shell-model calculations have generated transition matrix elements for this nucleus. Referring to Table 3 (5), the agreement between theory and experiment is excellent in most cases. The MSDI and FPSDI calculations of Glaudemans, et. al. and Wildenthal, et. al. are very similar and reproduce the data well, while the intermediate coupling calculation of Castel, et. al. is in somewhat worse agreement with experiment. The reduced widths determined in this experiment are shown in Table 2 and confirm the agreement between theory and experiment in every particular. For the nucleus ^{33}S current shell model theories work very well.

B. Conclusion

This work has shown that the $(\vec{d}, p\gamma)$ is a powerful tool for extracting information about electromagnetic transition strengths. As an example, in the case of ^{35}S this work has yielded M2 matrix element measurements for 3 levels (see Table 2), one of which was not measurable by other means.

Table 3. A comparison of experimental and theoretical work on ^{33}S. Glaudemans, et. al. and Wildenthal, et. al. made a MSDI shell model calculation, while Castel, et. al. made an intermediate coupling calculation.

			M^2 (W.u.)				
			EXPERIMENTAL		THEORETICAL		
E_x	J^π	Type	this work	ref. [5])	Glaudemans, et. al.	Wildenthal, et. al.	Castel, et. al.
841	$1/2^+$	M1		3×10^{-2}	3.1×10^{-2}	6.3×10^{-2}	4×10^{-4}
		E2		6	5	3.7	0.2
1968	5/2	M1	2×10^{-2}	1.7×10^{-2}	1.7×10^{-2}	6.8×10^{-2}	7×10^{-3}
		E2	2.4	5.6	8.7	5.9	12.4
2314	3/2	M1	3×10^{-3}	3.6×10^{-3}	2×10^{-3}	8×10^{-3}	4×10^{-5}
		E2	0.34	0.24	2.6	2.5	5.1
2868	(5/2)	M1	4×10^{-2}	3.9×10^{-2}	0.2	7×10^{-2}	4.5×10^{-2}
		E2	0.19	0.16	2.2	2.1	0.15

Referring to Table VIII in Endt and van der Leun (64) reveals that only five M2 strengths have been compiled. This ^{35}S work represents a significant increase in the body of experimental evidence on these transitions.

As stated at the outset, these measurements represent one of the first applications of polarized beams to γ-ray angular correlation work. In all cases where comparison data from other authors has been available agreement has been good. It is felt however that the experimental apparatus requires some additional refinement, something that will develop with further use. For example, some problems with isotropy were encountered in the original trial measurements that turned out to be related to phototube voltages, gains, etc. Some scattering of the data points of some correlation measurements that were somewhat larger than the error bars would have predicted implies that the γ-ray detection system requires some additional refinement. Further work will iron out these problems, with the result that future angular correlation fits will be improved.

This work has provided much new data that will allow the testing and extension of shell model theory to more of the s-d shell. Angular correlations provide experimental evidence of nuclear properties which are very sensitive tests of shell model theories. The use of the polarized beam has greatly enhanced the utility of the large number of possible (d,pγ) reactions in obtaining information about electromagnetic properties. It is felt that the disadvantage of the $(\vec{d},p\gamma)$ reaction relative to the $(\alpha,n\gamma)$ reaction for

angular correlation measurements---the requirement that two separate angular correlations be measured and combined---- is outweighed by the advantages afforded by detecting charged particles, where individual proton groups can be distinguished and feeding effects eliminated.

In closing, it should be noted that the polarized ion source is a very elegant instrument and its application to Method II angular correlations in no way exhausts its possibilities in future γ-ray work. More subtle and difficult experiments involving (for example) γ-ray polarization experiments and out-of-(reaction)plane correlations yielding parity and reaction mechanism information are made possible by the high performance and versatility of current polarized ion sources. These possibilities are barely beginning to be explored and should be of great importance in the future.

Chapter V

APPENDIX

The following is taken from the book Polarization Phenomena in Nuclear Reactions, edited by H. H. Barschall and W. Haeberli (U. of Wisc. Press, Madison, Wisc., 1970). One of the purposes of this symposium was to agree on standard conventions for the description of polarization experiments. The "Madison Convention" is the result.

I

Polarization effects involving spin-one particles should be described either by spherical tensor operators τ_{kq}, with normalization given by $Tr(\tau_{kq}\tau^{\dagger}_{k'q'}) = 3\delta_{kk'}\delta_{qq'}$, or by Cartesian operators S_i,

$$(3/2)(S_iS_j+S_jS_i)-2\delta_{ij}\ (i=x,y,z)$$

S_i denotes the usual spin-one angular momentum operators.

II

The state of spin orientation of an assembly of particles, referred to as polarization, should be denoted by the symbol t_{kq}(spherical) or p_i, p_{ij} (Cartesian). These quantities should be referred to a right-handed coordinate system in which the positive z-axis is along the direction of momentum of

the particles, and the positive y-axis is along $\vec{k}_{in} \times \vec{k}_{out}$ for the nuclear reaction which the polarized particles initiate, or from which they emerge.

III

Terms used to describe the effect of initial polarization of a beam or target on the differential cross section for a nuclear reaction should include the modifiers analyzing or efficiency, and should be denoted by T_{kq}(spherical) or A_i, A_{ij}(Cartesian). These quantities should be referred to a right-handed coordinate system in which the positive z-axis is along the beam direction of the incident particles and the y-axis is along $\vec{k}_{in} \times \vec{k}_{out}$ for the reaction in question.

IV

In the expression for a nuclear reaction A(b,c)D an arrow placed over a symbol denotes a particle which is initially in a polarized state or whose state of polarization is meosured.

o o o o o o o o o o o o o

In discussing polarization effects involving spin-one particles, either Cartesian tensors (as given by Goldfarb (Nucl. Phys. 7(1958)622)) or spherical tensors (as given by Lakin (Phys. Rev. 98(1955)139)) should be used. The two sets of tensor operators are given below in terms of the spin-one angular momentum operators and the unit matrix.

$$1 = \begin{vmatrix} 1 & 0 & 0 \\ 0 & 1 & 0 \\ 0 & 0 & 1 \end{vmatrix} ; \; S_x = (1/\sqrt{2}) \begin{vmatrix} 0 & 1 & 0 \\ 1 & 0 & 1 \\ 0 & 1 & 0 \end{vmatrix} ; \; S_y = (1/\sqrt{2}) \begin{vmatrix} 0 & -i & 0 \\ i & 0 & -i \\ 0 & i & 0 \end{vmatrix} ; \; S_z = \begin{vmatrix} 1 & 0 & 0 \\ 0 & 0 & 0 \\ 0 & 0 & -1 \end{vmatrix}$$

Spherical

$\tau_{00} = 1$

$\tau_{10} = (\sqrt{3}/2) S_z$

$\tau_{1\pm1} = \mp (1/2)\sqrt{3}(S_x \pm i S_y)$

$\tau_{20} = (1/\sqrt{2})(3S_z^2 - 2)$

$\tau_{2\pm1} = \mp (1/2)\sqrt{3}((S_x \pm i S_y)S_z + S_z(S_x \pm i S_y))$

$\tau_{2\pm2} = (1/2)\sqrt{3}(S_x \pm i S_y)^2$

In general, the τ_{kq} satisfy

$\tau_{kq} = (-1)^q \tau_{k-q}$

Cartesian

$p_x = S_x$

$p_y = S_y$

$p_z = S_z$

$p_{xx} = 3S_x^2 - 2$

$p_{yy} = 3S_y^2 - 2$

$p_{zz} = 3S_z^2 - 2$

$p_{xy} = (3/2)(S_x S_y + S_y S_x)$

$p_{xz} = (3/2)(S_x S_z + S_z S_x)$

$p_{yz} = (3/2)(S_y S_z + S_z S_y)$

Note that $p_{zz} = \sqrt{2}\, \tau_{20}$

LIST OF REFERENCES

References

1. J. A. Becker, et. al. Phys. Rev. 146(1966)761

2. M. Bini, P. G. Bizetti, A. M. Bizetti-Sona, Nuovo Cim. 12A no. 1(1972)215

3. F. Brandolini, et. al., Nuovo Cim. Lett. 2 (1969)600

4. F. Brandolini, C. Signorini, P. Kusstatscher, Nucl. Inst. Meth. 91(1971)341

5. P. E. Carr, D. C. Bailey, J. L. Durrell, L. L. Green, A. N. James, J. S. Sharpey-Schafer, D. A. Viggers, J. Phys. A. 6(1973)685

6. J. E. Cummings, U. Microfilms Ord. 70-17783

7. J. E. Cummings, D. J. Donahue, Nucl. Phys. A142(1970)609

8. J. E. Cummings, D. J. Donahue, Phys. Rev. C2(1970)942

9. A. W. Dalton, G. Parry, H. D. Scott, NPRL preprint (1961)

10. J. Dubois, Nucl. Phys. A117(1968)533

11. P. M. Endt, C. H. Paris, Phys. Rev. 110(1958)89

12. A. Grave, J. R. Lien, L. Rasmussen, G. E. Sandvik, E. R. Cosman, Nucl. Phys. A162(1971)593

13. R. G. Hirko, A. D. W. Jones, Nucl. Phys. A192(1972)329

14. R. W. Kavanaugh, J. C. Mardinger, N. Schultz, Nucl. Phys. A146(1970)410

15. J. Kopecky, E. Warming, Nucl. Phys. A127(1969)385

16. H. G. Leighton, A. C. Wolff, Nucl. Phys. A151(1970)71

17. M. C. Mermaz, et. al., Phys. Rev. C4(1971)1778

18. W. R. McMurray, Ann. Rept. SUNI-14

19. G. van Middlekoop, G. A. P. Engelbertink, Nucl. Phys. A138(1969)601

20. G. van Middlekoop, H. Gruppelaar, Nucl. Phys. 80(1966)321

21. J. M. O'Dell, R. W. Krone, F. W. Prosser, Jr. , Nucl. Phys. 82 (1966)574

22. C. E. Ragan, III, C. E. Moss, R. V. Poore, N. R. Roberson, G. E. Mitchell, D. R. Tilley, Phys. Rev. 188 (1969)1806

23. M. Toulemonde, N. Schultz, Nucl. Phys. A181 (1972)273

24. J. G. van der Baan, H. G. Leighton, Nucl. Phys. A170(1971)607

25. K. S. Burton, Univ. Microfilms No. 71-8435

26. K. S. Burton, L. C. McIntyre, Jr. , Nucl. Phys. A154(1970)551

27. D. J. Donahue, J. D. McCullen, L. C. McIntyre, Jr. , U. Arizona Progress Report 1970

28. R. M. Freeman, R. Faerber, M. Toulemonde, A. Gullman, Nucl. Phys. A197(1972) 529

29. G. I. Harris, F. W. Prosser, Jr. , Bull. Am. Phys. Soc. 15 (1970)1665

30. Th. W. van der Mark, L. K. ter Veld, Nucl. Phys. A181(1972)196

31. C. E. Moss, Nucl. Phys. A131(1969)235

32. F. W. Prosser, Jr. , G. I. Harris, Phys. Rev. C4(1971)1611

33. L. K. ter Veld, Th. W. van der Mark, Phys. Rev. 173 (1968)1101

34. B. Vignon, FRNC-TH-275

35. L. C. Biedenharn, G. B. Arfken, M. E. Rose, Phys. Rev. 83(1951)586

36. E. K. Warburton, H. J. Rose, Phys. Rev. 109 (1958)1199

37. J. O. Newton, Ph. D. dissertation, unpublished, U. of Cambridge(1952)

38. A. A. Debenham, G. R. Satchler, Particles and Nuclei, 3(1972)117

39. S. Devons, L. J. B. Goldfarb, Handbuch der Physik, v. 42(1957)

40. L. J. B. Goldfarb, Nucl. Phys. 7(1958)622

41. A. E. Litherland, A. J. Ferguson, Can. J. Phys. 39(1961)788

42. J. D. McCullen, R. G. Seyler, Nucl. Phys. A139(1969)203

43. H. J. Rose, D. M. Brink, Rev. Mod. Phys. 39(1967)306

44. F. Rybicki, T. Tamura, G. R. Satchler, Nucl. Phys. A146(1970)659

45. H. H. Barschall, W. Haeberli, Polarization Phenomena in Nuclear Reactions, (U. Wisc. Press, Madison, Wisc. 1970)

46. T. B. Clegg, G. A. Bissinger, W. Haeberli, P. A. Quin, Proceedings of 3rd Int'l Conf. on Polarization Phenomena in Nuclear Reactions, ed. by H. H. Barschall and W. Haeberli (U. Wisc. Press, Madison, Wisc. 1970)

47. G. G. Ohlsen, J. L. McKibben, G. P. Lawrence, P. W. Keaton, Jr., D. D. Armstrong, Phys. Rev. Lett. 27(1971)599

48. G. P. Lamaze, C. R. Gould, C. E. Moss, N. R. Roberson, D. R. Tilley, Nucl. Phys. A158(1970)43

49. B. Castel, K. W. C. Stewart, M. Harvey, Nucl. Phys. A162(1971)273

50. P. R. DeKock, P. W. M. Glaudemans, Phys. Lett. 34B(1971)280

51. P. W. M. Glaudemans, P. M. Endt, A. E. L. Dieperink, Ann. Phys. 63(1971)134

52. B. H. Wildenthal, J. B. McGrory, E. C. Halbert, H. D. Graber, Phys. Rev. C4 (1971)1708

53. A. E. L. Dieperink, P. J. Brussaard, Nucl. Phys. A128(1969)34

54. F. C. Erne, Nucl. Phys. 84(1966)91

55. P. W. M. Glaudemans, G. Weichers, P. J. Brussaard, Nucl. Phys. 56(1964)529, 548

56. G. I. Harris, J. J. Perrizo, Phys. Rev. C2 (1970)1347

57. S. Maripuu, G. A. Hokken, Nucl. Phys. A141(1970)481

58. D. D. Watson, F. D. Lee, Phys. Lett. 25B(1967)472

59. G. Weichers, P. J. Brussaard, Nucl. Phys. 73(1965)604

60. B. H. Wildenthal, P. W. M. Glaudemans, Nucl. Phys. A108(1968)49

61. B. H. Wildenthal, E. C. Halbert, J. B. McGrory, T. T. S. Kuo, Phys. Lett. 32B(1970)339

62. B. H. Wildenthal, J. B. McGrory, P. W. M. Glaudemans, Phys. Rev. Lett. 26 (1971)96

63. B. H. Wildenthal, J. B. McGrory, E. C. Halbert, P. W. M. Glaudemans, Phys. Lett. 27B (1968)611

64. P. M. Endt, C. van der Leun, Nucl. Data Tables, to be published

65. D. J. Church, private communication

66. A. R. Poletti, E. K. Warburton, Phys. Rev. 137 (1965)B595

67. P. B. Smith, Can. J. Phys. 42(1964)1101

68. C. R. Gould, R. O. Nelson, J. R. Williams, D. R. Tilley, J. D. Hutton, N. R. Roberson, C. E. Busch, T. B. Clegg, Phys. Rev. Lett. 30(1973)298

69. A. H. Wapstra, G. J. Nijgh, R. van Lieshout, Nuclear Spectroscopy Tables, (North-Holland Publ. Co., Amsterdam, 1959)

BIOGRAPHY

James David Hutton

Personal:	Born 17 June 1946, Indianapolis, Indiana
	Married
Education:	B. A. in Physics, Rice University (1968)
	M. A. in Physics, Duke University (1971)
Posistions:	Teaching Assistant, Duke University, 1969-1970
	Research Assistant, Duke University, 1970-1974
Membership:	American Physical Society

Abstracts:

1. A Study of Low-Lying Levels in ^{59}Ni (with N. R. Roberson, C. R. Gould, and D. R. Tilley) Nucl. Phys. A206(1973)298
2. Application of Polarized Deuterons in (d,py) Angular Correlation Measurements (with C. R. Gould, R. O. Nelson, J. R. Williams, D. R. Tilley, N. R. Roberson, C. E. Busch, and T. B. Clegg) Phys. Rev. Lett. 30(1973)403